Estimating nonaqueous phase liquid spatial variability using partitioning tracer higher temporal moments

James W. Jawitz,[1] Michael D. Annable,[2] George G. Demmy,[3] and P. S. C. Rao[4]

Received 14 March 2002; revised 26 November 2002; accepted 21 February 2003; published 29 July 2003.

[1] The use of interwell partitioning tracers to quantify the amount of nonaqueous phase liquid (NAPL) in porous media has been demonstrated in several laboratory and field tests. The primary emphasis of work to date has been on the use of first temporal moments of tracer breakthrough curve (BTC) data to estimate the average NAPL saturation. Here we extend the data analysis to the use of tracer BTC second and third temporal moments to estimate the statistical parameters characterizing the NAPL spatial distribution. In particular, we examine the fraction *f* of the streamlines that contain NAPL and the mean and standard deviation of the distribution of streamline trajectory-average NAPL saturations. Two models are presented based on discretizing tracer swept volumes into contaminated and uncontaminated zones. The models are applied to data from three-dimensional numerical simulations, two-dimensional flow laboratory experiments, and field tests at two sites (Hill Air Force Base, Utah, and a dry cleaner in Jacksonville, Florida). For all cases considered here, good agreement was found between expected (measured) and estimated values of *f*, the fraction of the tracer swept zone that contained NAPL. The effects of nonlinear and nonequilibrium partitioning as well as correlations between NAPL saturation and saturated hydraulic conductivity are also considered. *INDEX TERMS:* 1829 Hydrology: Groundwater hydrology; 1831 Hydrology: Groundwater quality; 1832 Hydrology: Groundwater transport; *KEYWORDS:* groundwater hydrology, groundwater quality, groundwater transport

Citation: Jawitz, J. W., M. D. Annable, G. G. Demmy, and P. S. C. Rao, Estimating nonaqueous phase liquid spatial variability using partitioning tracer higher temporal moments, *Water Resour. Res.*, *39*(7), 1192, doi:10.1029/2002WR001309, 2003.

1. Introduction

[2] The design of effective subsurface remediation strategies requires knowledge of both the amount and spatial distribution of the contaminants present. Interwell partitioning tracers have been used at both the laboratory and field scales to detect and quantify nonaqueous phase liquid (NAPL) contaminants in the subsurface [*Jin et al.*, 1995; *Nelson and Brusseau*, 1996; *Annable et al.*, 1998; *Jawitz et al.*, 1998c, 2000; *Falta et al.*, 1999; *Cain et al.*, 2000; *Meinardus et al.*, 2002]. The partitioning tracer methodology involves the selection of tracers that partition into the NAPL phase with predictable or measurable relationships. A suite of these tracers is injected into a steady-state flow field at one or more injection wells and recovered down gradient at extraction wells. Tracer partitioning is manifested as delayed or retarded transport observed in tracer breakthrough curves (BTCs). The degree of separation can be related to the quantity of NAPL present in the zone swept by the tracers.

[3] To date, the interpretation of partitioning tracer data has been restricted to analyses of BTC first temporal moments for the characterization of domain-average NAPL saturation, enabling estimation of the total NAPL volume within the tracer swept volume. The determination of the spatial distribution of the NAPL mass within the flow domain requires either intensive soil core sampling [e.g., *Rao et al.*, 1997; *Jawitz et al.*, 1998c, 2000; *Meinardus et al.*, 2002] or partitioning tracer characterization at multiple sampling locations [*Sillan et al.*, 1998; *Jawitz et al.*, 1999]. *James et al.* [1997] and *Zhang and Graham* [2001] presented inverse modeling stochastic algorithms for estimating NAPL spatial distributions using partitioning tracer data collected from a network of multilevel samplers.

[4] Here, we describe the use of partitioning tracers and the method of temporal moments [e.g., *Valocchi*, 1985] to characterize the spatial distribution of NAPLs in porous media using only one sampling location. Our approach is based on the Lagrangian conceptualization of flow fields as collections of noninteracting streamtubes, wherein solute transport can be described in terms of trajectories along streamlines. Along each streamline, nonreactive tracers provide integrative measures of the hydrodynamic heterogeneity of the media between tracer injection and monitoring points, and reactive (partitioning) tracers provide similar integrative information about the combined influences of hydrogeology and reactive surfaces (NAPL) [e.g., *Cvetkovic et al.*, 1998]. This Lagrangian approach is combined with a binary model, wherein it is assumed that

[1]Soil and Water Science Department, University of Florida, Gainesville, Florida, USA.
[2]Department of Environmental Engineering Sciences, University of Florida, Gainesville, Florida, USA.
[3]Layton Graphics, Inc., Atlanta, Georgia, USA.
[4]School of Civil Engineering, Purdue University, West Lafayette, Indiana, USA.

0043-1397/03/2002WR001309

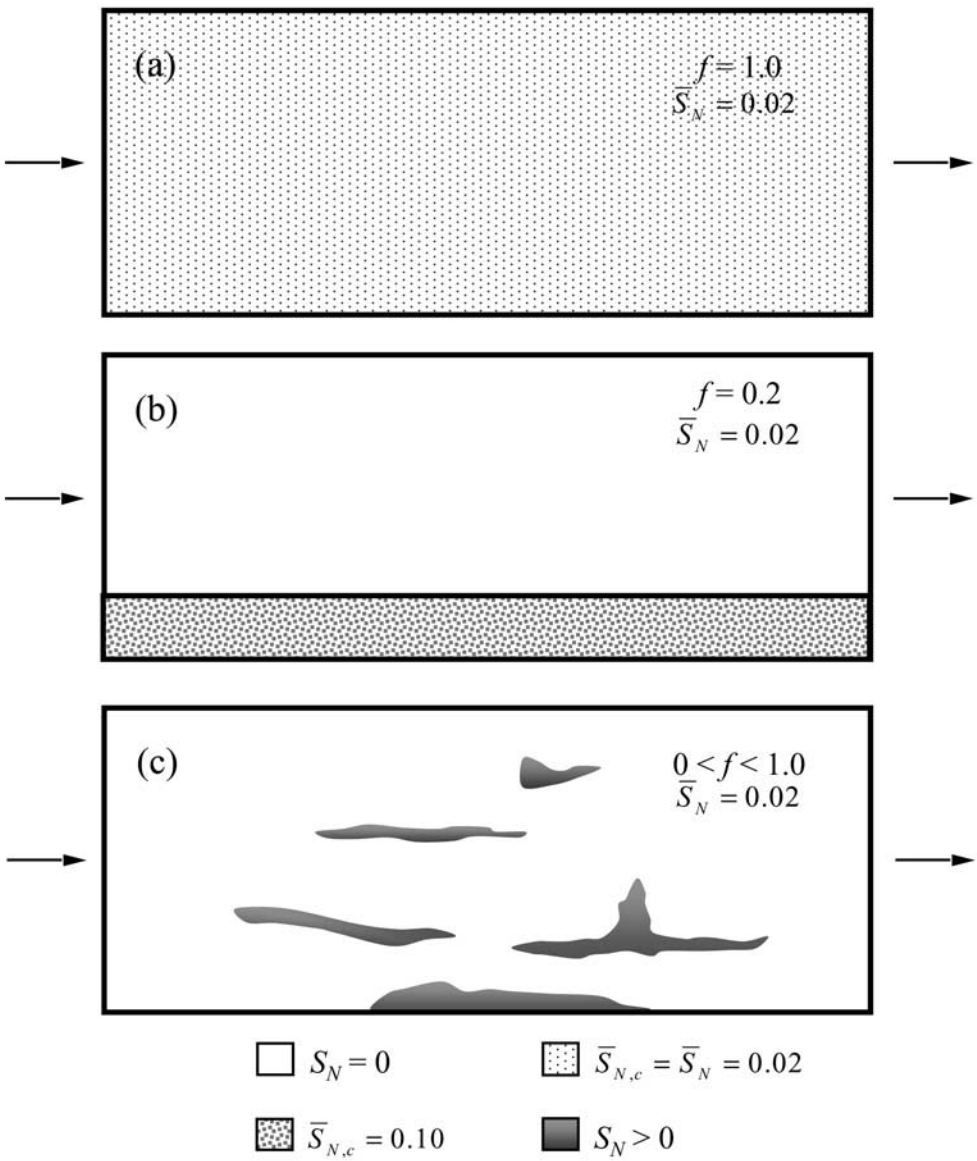

Figure 1. Comparison of NAPL distribution models: (a) homogeneous, (b) homogeneous binary model where a fraction of the horizontal trajectories are contaminated with uniform trajectory-average saturations, and (c) distributed binary model where a fraction of the trajectories exhibit a distribution of trajectory-average saturations. Note that the domain-average NAPL saturation is equal for all three cases shown.

some fraction of the streamlines transecting a domain are uncontaminated and the NAPL saturation in the remaining fraction f can be represented either as a homogeneous value, or as a distribution of saturations. *Soerens et al.* [1998] also considered homogeneous and distributed binary models of NAPL distribution in relation to aqueous dissolution. The goal of the binary models described here is to express partitioning tracer moments in terms of nonpartitioning tracer moments and parameters that describe the NAPL spatial distribution, which can be estimated from the measured tracer moments.

[5] Four spatially descriptive definitions of NAPL saturation (generally defined as the ratio of the volume of NAPL contaminants to the pore volume) are distinguished: (1) Local or point saturation, S_N, (2) Average saturation for the entire spatial domain, $\bar{S}_N$, (3) Average saturation for the contaminated fraction of the domain $\bar{S}_{N,c} = \bar{S}_N/f$, and (4) Trajectory-average saturation along a streamline, $\hat{S}_N$. The binary models of NAPL distribution, and these definitions of NAPL spatial structure are illustrated in Figure 1.

[6] First temporal moment analysis of partitioning tracer data enables estimation of $\bar{S}_N$ [e.g., *Jin et al.*, 1995]. The

homogeneous binary model extends partitioning tracer analysis to second moments [*Jawitz et al.*, 1998b], enabling estimation of both $\bar{S}_N$ and the fraction f of the streamlines in the domain that are contaminated. For heterogeneously distributed NAPLs, the streamlines that transect the contaminated zone exhibit a distribution of trajectory-average NAPL saturations, $\hat{S}_N$. The distributed binary model considers partitioning tracer first, second, and third temporal moments, enabling estimation of f and the mean and variance of the trajectory-average NAPL saturation distribution. The applicability of both the homogeneous and distributed binary models is explored here using numerical simulations, laboratory experiments, and field data. Laboratory and field results presented here are from extraction wells representing flux-averages over the screened interval; however, the methodology is equally applicable to tracer BTC data collected at smaller scales, such as multilevel samplers [e.g., *James et al.*, 1997; *Sillan et al.*, 1998].

[7] The binary approach is advantageous because contaminant source zones may include relatively large portions that do not contain NAPL. Establishing the fraction of tracer trajectories that are uncontaminated may be significant for the design of remediation systems such as in situ flushing [e.g., *Jawitz et al.*, 1998c, 2000; *Falta et al.*, 1999], where the remediation and tracer test hydraulic configurations (i.e., well pattern and flow rates) are similar. The delivery of remedial fluids to uncontaminated zones is both inefficient and expensive. Ascertaining the fraction of the swept zone that is uncontaminated may lead to the implementation of more efficient and less expensive remediation designs. For example, if it is known that a large fraction of the remedial fluids to be flushed through a contaminant source zone will not contact any NAPL, alternate well configurations or remedial technologies may be investigated.

[8] The presence of NAPL contaminants in the subsurface may affect the porous media hydraulic properties, altering the flow field. For example, flow bypassing may occur around regions of high NAPL saturations [*Soerens et al.*, 1998]. Consequently, the present approach is useful primarily for 'low' residual saturations where the media hydraulic properties are not significantly affected by the NAPL. In the laboratory and field experiments discussed here, the domain average NAPL saturations were considered low enough (the maximum value here is 0.063) that the effects of NAPL on the flow field were considered minor. Note that several other field studies have documented similarly low residual NAPL saturations [e.g., *Annable et al.*, 1998; *Falta et al.*, 1999; *Cain et al.*, 2000; *Meinardus et al.*, 2002]. The effects of flowing or mobile NAPLs were also not considered.

2. Theory

2.1. Transfer Function Approach

[9] *Jury* [1982] proposed modeling solute BTCs as lognormal travel time distributions as an alternative to the ADE. An advantage of this strategy is that parameters affecting solute travel time can be estimated without the constraint of describing the causative transport processes. The lognormal distribution is appropriate for many properties related to geologic media because the distribution originates from processes that involve multiplicative effects of independent random events, such as a sequence of particle breakages resulting in a distribution of particle sizes [*Aitchison and Brown*, 1957]. The logarithm of a product of random processes results in a sum of logarithms, which is normally distributed according to the central limit theorem. A lognormal random variable X is one for which $Y = \ln X$ is normally distributed with mean $\mu_{\ln X}$ and standard deviation $\sigma_{\ln X}$. If solute arrival time, t, is considered as a random variable, then the lognormal probability density function (PDF), $p(t)$, is described by the following equation:

$$p(t) = \frac{1}{\sqrt{2\pi}\sigma_{\ln t} t} \exp\left(-\frac{(\ln(t) - \mu_{\ln t})^2}{2\sigma_{\ln t}^2}\right), \quad t > 0, \sigma_{\ln t} > 0 \tag{1}$$

2.2. Method of Moments

[10] The method of moments is an effective technique for determining model parameters from measured data. The Nth temporal moment, M_N, of a distribution, $p(t)$, is defined:

$$M_N = \int_0^\infty t^N p(t) dt \tag{2}$$

The absolute moments of measured BTCs are calculated by replacing $p(t)$ in (2) with measured solute concentration values, $C(t)$. Normalized moments, m_N, are Nth absolute moments scaled to the zeroth moment. Model parameters are determined by equating measured moments, determined through numerical integration of measured data [e.g., *Haas*, 1996], with derived moment expressions, generating a system of N equations that can be solved for N model parameters.

[11] The following expression for the Nth normalized moment of a lognormal travel time distribution can be derived by substituting (1) into (2) and integrating [e.g., *Jury and Roth*, 1990]:

$$m_N = \exp\left(N\mu_{\ln t} + N^2\sigma_{\ln t}^2/2\right) \tag{3}$$

2.3. Partitioning Tracers

[12] Tracer retardation, R, is determined from the ratio of the mean arrival times (i.e., first normalized temporal moments) of the partitioning tracer, m_1^p, and the nonpartitioning tracer, m_1^{np}, both corrected for the solute pulse injection duration, t_0:

$$R = \frac{m_1^p - \frac{t_0}{2}}{m_1^{np} - \frac{t_0}{2}} \tag{4}$$

Following *Jin et al.* [1995], we relate retardation for the entire domain, R_T, to the average NAPL saturation in the system, $\bar{S}_N$, and the NAPL-water partitioning coefficient, K_N:

$$R_T = 1 + \frac{K_N \bar{S}_N}{1 - \bar{S}_N} \tag{5}$$

This relation requires the assumption that tracer partitioning follows a linear, reversible isotherm.

2.4. NAPL Spatial Distribution Models

2.4.1. Excess Spreading of Tracer BTCs

[13] A flux-averaged BTC measured from the transport of an instantaneously injected nonpartitioning tracer through a porous medium will exhibit some degree of spreading, characterized by the second moment, that is representative of the degree of heterogeneity of the media. The transport of a partitioning tracer through the same medium will be retarded according to (5) and the measured BTC will exhibit a greater degree of spreading than that of the nonpartitioning tracer. For example, if transport is adequately described by the advection-dispersion equation (ADE) and partitioning is both instantaneous and linear, the partitioning tracer second moment, m_2^p, can be expressed as m_2^{np} multiplied by R^2 [e.g., *Valocchi*, 1985]. Any BTC spreading beyond that expected based on m_2^{np} and R can be considered as 'excess' spreading.

[14] A nonhomogeneous NAPL distribution can contribute to partitioning tracer BTC excess spreading that is manifested in the higher moments (i.e., $N > 1$). The goal of this work is to use nonpartitioning and partitioning tracer moments to infer properties of the spatial distribution of NAPL contaminants based on the concept of excess spreading. However, nonuniformly distributed NAPL is not the only cause of partitioning tracer BTC excess spreading. Confounding effects include nonequilibrium partitioning [*Valocchi*, 1985], nonlinear partitioning [*Wise et al.*, 1999], and a correlation between S_N and hydraulic conductivity, K [e.g., *Valocchi*, 1989]. The significance of correlations between S_N and K was evaluated in this study with numerical simulations, while nonlinear and nonequilibrium effects were evaluated in laboratory experiments.

2.4.2. Binary Model Framework and Assumptions

[15] Consider a multidimensional flow field that is resolved into a collection of noninteracting streamtubes. A fraction f of the total number of streamtubes in the domain is assumed to be contaminated, while the remaining fraction (1-f) of the streamtubes is uncontaminated. At low residual saturations, nonpartitioning tracer transport is assumed to be identical in the contaminated and uncontaminated regions, assuming. Thus, $m_{N,c}^{np} = m_{N,uc}^{np} = m_{N,T}^{np}$, where the subscripts, c, uc, and T refer to contributions from the contaminated, uncontaminated, and total domain fractions, respectively. Because of this equivalence, these subscripts will be dropped when referring to the nonpartitioning tracer moments hereafter.

[16] Partitioning tracer retardation in the contaminated fraction of the domain, R_c, is related to $\bar{S}_{N,c}$ as in (5):

$$R_c = 1 + \frac{K_N \bar{S}_{N,c}}{1 - \bar{S}_{N,c}} \tag{6}$$

Combination of (5) and (6) results in the following relation between total retardation and contaminated zone retardation:

$$R_T = (1 - \phi) + \phi R_c \tag{7}$$

where

$$\phi = \frac{f - \bar{S}_N}{1 - \bar{S}_N} \tag{8}$$

Application of the definition of R from (4) (i.e., the ratio of partitioning and nonpartitioning tracer first moments) to R_T and R_c, and substitution into (7) results in

$$m_{1,T}^p = (1 - \phi) m_1^{np} + \phi m_{1,c}^p \tag{9}$$

Thus, the partitioning tracer normalized moment from the total domain can be obtained through the superposition of moments from the uncontaminated and contaminated fractions. Note that (9) reflects that for a partitioning tracer that does not react with the media, transport through the uncontaminated region is identical to that of the nonpartitioning tracer, such that $m_{N,uc}^p = m_N^{np}$. The results from (9) may be generalized for the Nth moment as:

$$m_{N,T}^p = (1 - \phi) m_N^{np} + \phi m_{N,c}^p \tag{10}$$

Note from (8) that as $\bar{S}_N$ approaches zero, $\phi \rightarrow f$ and the superposition relationship (10) becomes a fractional sum of the contributions from the uncontaminated and contaminated portions of the domain.

[17] *Jawitz* [1999] developed binary model equations, after those of *Soerens et al.* [1998], that account for the effects of NAPL on media properties and flow bypassing; however, it was found that because of the relatively low NAPL saturations considered here, these effects were minor (consideration of bypassing in the laboratory experiments discussed below resulted in corrections to f of approximately 2–3%). Therefore, these effects will not be considered further here.

2.4.3. Homogeneous Binary Model

[18] In this model, a fraction f of the streamtubes within the domain is assumed to be homogeneously contaminated with NAPL at saturation $\bar{S}_{N,c} = \bar{S}_N / f$ (Figure 1b). In many real systems, NAPLs are non-homogeneously distributed within a streamtube, where individual trajectories may intercept a number of contaminated and uncontaminated zones between injection and extraction points. Here, we consider only the trajectory-average NAPL saturation, which is independent of the location of the NAPL along the trajectory. It is assumed that each streamtube is independent and NAPL-water partitioning is instantaneous and linear. Four parameters are then required to describe reactive solute transport through this binary system: Two that describe the nonpartitioning solute behavior ($\mu_{\ln t,np}$ and $\sigma_{\ln t,np}$ for the lognormal distribution model), and two that describe the NAPL saturation distribution (f and $\bar{S}_{N,c}$). These four parameters may be estimated using four moment equations (two each for the nonpartitioning and partitioning tracers).

[19] By considering the tracer arrival times in (4) as random variables and combining with (6), partitioning tracer arrival time can be expressed as a function of nonpartitioning tracer arrival time and $\bar{S}_{N,c}$:

$$t_{p,c} = t_{np} + K_N \bar{S}_c t_{np} - K_N \bar{S}_c \frac{t_0}{2} \tag{11}$$

where $\bar{S}_c = \bar{S}_{N,c} / (1 - \bar{S}_{N,c})$ and $\bar{S}_c$, K_N, and t_0 are constants for each streamtube. The Nth partitioning tracer moment for

the contaminated portion of the domain can then be determined by taking the expected value of both sides of (11):

$$m^p_{N,c} = \mathrm{E}\left[t^N_{p,c}\right] = \mathrm{E}\left[\left(t_{np} + K_N \bar{S}_N t_{np} - K_N \bar{S}_c \frac{t_0}{2}\right)^N\right] \tag{12}$$

where the expected value notation, $\mathrm{E}[X^N]$, is equivalent to the Nth moment of X. Expansion of (12) and incorporation into (10) results in the homogeneous binary model equations for total-domain partitioning tracer moments, which are expressed in terms of nonpartitioning tracer moments and NAPL spatial distribution parameters:

$$m^p_{1,T} = (1-\phi)m^{np}_1 + \phi\left[m^{np}_1 + K_N \bar{S}_c m^{np}_1 - K_N \bar{S}_c \frac{t_0}{2}\right] \tag{13}$$

$$m^p_{2,T} = (1-\phi)m^{np}_2 + \phi\left[\left(1 + 2K_N\bar{S}_c + K^2_N \bar{S}^2_c\right)m^{np}_2 - \left(K_N \bar{S}_c t_0 + K^2_N \bar{S}^2_c t_0\right)m^{np}_1 + K^2_N \bar{S}^2_c \frac{t^2_0}{4}\right] \tag{14}$$

2.4.4. Distributed Binary Model

[20] It is perhaps more likely that NAPL saturations within a contaminated zone will be distributed heterogeneously, rather than in a homogeneous fashion (Figure 1c). Here, the lognormal PDF is used to describe both the travel time and trajectory-average NAPL content distributions. Using this approach, five parameters are now required to describe reactive solute transport through the system: Two that describe the nonpartitioning solute behavior ($\mu_{\ln t,np}$ and $\sigma_{\ln t,np}$), one that quantifies the contaminated fraction of the domain (f), and two that describe the NAPL saturation distribution within the contaminated fraction ($\mu_{\ln \hat{S}}$ and $\sigma_{\ln \hat{S}}$). These five unknown parameters may be estimated using five moment equations (two for the nonpartitioning tracer and three for the partitioning tracer).

[21] Following (5) and (6), $R_i = 1 + K_N \hat{S}_N/(1 - \hat{S}_N)$ is the retardation in a streamtube containing NAPL for the distributed model. Thus, analogous to the homogeneous binary model, the contaminated zone partitioning tracer moments can be expressed as:

$$m^p_{N,c} = \mathrm{E}\left[t^N_{p,c}\right] = \mathrm{E}\left[\left(t_{np} + K_N \hat{S} t_{np} - K_N \hat{S} \frac{t_0}{2}\right)^N\right] \tag{15}$$

where now both t_{np} and $\hat{S} = \hat{S}_N/(1 - \hat{S}_N)$ are lognormal random variables that may be correlated. The trajectory-average "NAPL content" $\hat{S}$ [e.g., *James et al.*, 1997], rather than the NAPL saturation $\bar{S}_N$, was assumed to be lognormally distributed because the range for both NAPL content and lognormal distributions is $[0,\infty]$ while the range for NAPL saturation is [0,1].

[22] Solution of (15) requires consideration of the product of correlated lognormal distributions. If $Z = X^a Y^b$ is a product of lognormal random variables, then $\ln Z = a\ln X + b\ln Y$ is a sum of normal random variables, which is itself normal. Thus, Z is lognormal with

$$\mu_{\ln Z} = a\mu_{\ln X} + b\mu_{\ln Y}, \sigma^2_{\ln Z} = a^2\sigma^2_{\ln X} + b^2\sigma^2_{\ln Y} + 2ab\rho_{X,Y}\sigma_{\ln X}\sigma_{\ln Y} \tag{16}$$

where $\rho_{X,Y}$ is the correlation coefficient between X and Y. The correlation coefficient quantifies the degree of interrelation between two random variables and is defined:

$$\rho_{X,Y} = \frac{E\left[\left(X - m^X_1\right)\left(Y - m^Y_1\right)\right]}{\sigma_{\ln X}\sigma_{\ln Y}} \tag{17}$$

Substituting (16) into (3) and simplifying results in:

$$\mathrm{E}\left[X^a Y^b\right] = m^X_a m^Y_b \exp\left(ab\rho_{X,Y}\sigma_{\ln X}\sigma_{\ln Y}\right) \tag{18}$$

Expansion of (15), using (18), and incorporation into (10) results in the distributed binary model equations for total-domain partitioning tracer moments, which are expressed in terms of nonpartitioning tracer moments and NAPL spatial distribution parameters:

$$m^p_{1,T} = (1-\phi)m^{np}_1 + \phi\left[m^{np}_1 + K_N m^{\hat{S}}_1 m^{np}_1 \gamma - m^{\hat{S}}_1 K_N \frac{t_0}{2}\right] \tag{19}$$

$$m^p_{2,T} = (1-\phi)m^{np}_2 + \phi\left[\left(1 + 2K_M m^{\hat{S}}_1\gamma^2 + K^2_N m^{\hat{S}}_2\gamma^4\right)m^{np}_2 - \left(K_N m^{\hat{S}}_1 t_0\gamma + K^2_N m^{\hat{S}}_2 t_0\gamma^2\right)m^{np}_1 + K^2_N m^{\hat{S}}_2 \frac{t^2_0}{4}\right] \tag{20}$$

$$m^p_{3,T} = (1-\phi)m^{np}_3 + \phi\left[\left(1 + 3K_N m^{\hat{S}}_1\gamma^3 + 3K^2_N m^{\hat{S}}_2\gamma^6 + K^3_N m^{\hat{S}}_3\gamma^9\right)m^{np}_3 - \left(K_N m^{\hat{S}}_1 \frac{t_0}{2}\gamma^2 + K^2_N m^{\hat{S}}_2 t_0\gamma^4 + K^3_N m^{\hat{S}}_3 \frac{t_0}{2} + K^2_N m^{\hat{S}}_2 \frac{t^2_0}{2}\gamma^2 + K^3_N m^{\hat{S}}_3 \frac{t^2_0}{4}\gamma^3\right)3m^{np}_1 - K^3_N m^{\hat{S}}_3 \frac{t^3_0}{8}\right] \tag{21}$$

The correlation terms in (19)–(21) have been simplified with the notation $\gamma = \exp(\rho_{t,\hat{S}}\sigma_{\ln t,np}\sigma_{\ln \hat{S}})$.

[23] Note that the above moment equations account for tracer rectangular pulse inputs of duration t_0; however, the equations for both models are significantly simplified for Dirac inputs (i.e., $t_0 \to 0$). The laboratory and field results presented below were determined in consideration of actual t_0 values (the simulations were conducted with instantaneous tracer release). For these data, ignoring t_0 and using the simpler forms of the equations for both models resulted in errors of approximately 1% and 10% in the estimated f and $\bar{S}_N$ values, respectively.

2.5. Parameter Estimation

[24] The binary models described above express tracer moments in terms of parameters that describe the NAPL spatial distribution. Thus, moments of measured tracer BTCs may be used to estimate these parameters. First, solution of (3) for $N = \{1,2\}$ allows the lognormal PDF parameters describing nonpartitioning tracer transport to be written in terms of the first two normalized temporal moments from a measured BTC as follows:

$$\mu_{\ln t,np} = 2\ln\left(m^{np}_1\right) - \frac{\ln\left(m^{np}_2\right)}{2} \tag{22}$$

$$\sigma^2_{\ln t,np} = \ln\left(m^{np}_2\right) - 2\ln\left(m^{np}_1\right) \tag{23}$$

Table 1. Actual and Estimated $\hat{S}$ Distribution Model Parameters From Three-Dimensional Particle Tracking Simulations[a]

	$\mu_{\ln \hat{S}}$	$\sigma_{\ln \hat{S}}$	$\rho_{t,\hat{S}}$	RMSD ($\times 10^{-5}$)
$\sigma_{\ln K}^2 = 0.2$, $b = 0$				
Actual	−2.95 ± 3.00E-4	0.123 ± 0.002	0.016 ± 0.021	
Model fit	−2.96 ± 0.009	0.153 ± 0.038	−0.002 ± 0.003	6.65 ± 2.10
$\sigma_{\ln K}^2 = 0.2$, $b > 0$				
Actual	−2.94 ± 6.10E-4	0.120 ± 0.003	−0.350 ± 0.010	
Model fit	−2.93 ± 0.011	0.117 ± 0.006	−0.361 ± 0.019	5.08 ± 3.52
$\sigma_{\ln K}^2 = 0.2$, $b < 0$				
Actual	−2.97 ± 5.5E-4	0.128 ± 0.002	0.369 ± 0.023	
Model fit	−2.97 ± 0.002	0.143 ± 0.022	0.350 ± 0.004	3.96 ± 1.37
Fit, $\rho_{t,\hat{S}} = 0.0$	−2.98 ± 0.008	0.225 ± 0.030	−0.001 ± 0.002	6.24 ± 2.16
$\sigma_{\ln K}^2 = 1.0$, $b = 0$				
Actual	−3.02 ± 0.008	0.321 ± 0.008	−0.009 ± 0.006	
Model fit	−2.98 ± 0.030	0.229 ± 0.068	0.0 ± 0.0	53.0 ± 32.5
$\sigma_{\ln K}^2 = 1.0$, $b > 0$				
Actual	−2.93 ± 0.010	0.301 ± 0.006	−0.347 ± 0.006	
Model fit	−2.93 ± 0.012	0.287 ± 0.018	−0.413 ± 0.044	14.6 ± 6.02
$\sigma_{\ln K}^2 = 1.0$, $b < 0$				
Actual	−3.10 ± 0.005	0.342 ± 0.009	0.317 ± 0.005	
Model fit	−3.10 ± 0.010	0.308 ± 0.034	0.341 ± 0.008	209 ± 349

[a]Values reported are mean and standard deviation for simulations conducted with different contaminated fractions, $f = \{0.1, 0.4, 0.6, 1.0\}$ and $\{0.25, 0.5, 0.75, 1.0\}$ for $\sigma_{\ln K}^2 = 0.2$ and 1.0, respectively. Model fits were determined using the binary distributed model (19)–(21). Reported RMSD values are between partitioning tracer actual and model-fit first three normalized temporal moments.

When the homogeneous binary model is assumed, the NAPL distribution parameters f and $\bar{S}_{N,c}$ are then determined from the tracer BTC moments by algebraic solution of (13) and (14). The application of (13) and (14) to other solute transport models such as the ADE is also valid, subject to the constraints of the given assumptions.

[25] For the distributed binary model, the parameters describing the NAPL saturation distribution (f, $\mu_{\ln \hat{S}}$, $\sigma_{\ln \hat{S}}$ and $\rho_{t,\hat{S}}$) are determined by solving (19)–(21) using the measured nonpartitioning and partitioning tracer moments. For uncorrelated cases ($\rho_{t,\hat{S}} = 0$), (19)–(21) may be solved algebraically; however, for correlated cases, algebraic solution of these equations is intractable. For the correlated cases considered here, model parameters were estimated by variable metric (Newton) regression where the root mean squared deviation (RMSD) between the measured partitioning tracer moments and those calculated from (19)–(21) was minimized:

$$\mathrm{RMSD} = \left[\frac{1}{p}\sum_{i=1}^{p}\left(\frac{m_i^m - m_i^c}{m_i^m}\right)^2\right]^{\frac{1}{2}} \tag{24}$$

where the superscripts m and c represent measured and computed moments, respectively, and p is the number of moments used.

2.6. Generating Model PDFs

[26] It is usually desirable to generate model BTCs for comparison with measured data following model parameter estimation from moment equations. The focus here is on representing nonpartitioning and partitioning tracer BTCs using lognormal distributions. For simple nonpartitioning tracer BTCs, model fits can be generated directly from (1) using the lognormal PDF parameters $\mu_{\ln t,np}$ and $\sigma_{\ln t,np}$ determined from (22) and (23).

[27] Under the binary NAPL distribution framework, partitioning tracer BTCs can be generated through the superposition of solutions of (1) for the uncontaminated and contaminated zones, as with the partitioning tracer moments in (10):

$$p(t_{p,T}) = (1-\phi)p(t_{p,uc}) + \phi p(t_{p,c}) \tag{25}$$

Again, transport through the uncontaminated region is assumed to be identical to that of the nonpartitioning tracer, such that $t_{p,uc} = t_{np}$. In the contaminated zone, (11) and (15) reveal $t_{p,c}$ to be equivalent to a sum of lognormal distributions for both the homogeneous and distributed binary models, where the constant terms in (11) are considered zero-variance distributions. The sum of N lognormal random variables has been demonstrated to be very closely approximated by a lognormal distribution, even for high-variance cases [*Schwartz and Yeh*, 1982; *Abu-Dayya and Beaulieu*, 1994]. Therefore, by subtracting the estimated fractional contribution of the uncontaminated zone from the total BTC moments in (10), the resulting moments, representative of tracer travel through only the contaminated zone, can be used with (22) and (23) to determine the lognormal PDF parameters $\mu_{\ln t,pc}$ and $\sigma_{\ln t,pc}$ for $t_{p,c}$. This approach was employed to generate model BTCs using (25) for the numerical simulations and laboratory experiments described below. Methods for generating model BTCs for the field experiments are discussed in a separate section below.

3. Numerical Simulations

[28] The utility of the binary model moment equations derived above was evaluated using three-dimensional numerical simulations of tracer transport in saturated porous media. The motivations for these simulations included: (1) Validating the binary model equations derived above, (2) Assessing the suitability of the excess spreading approach for estimating NAPL spatial distribution parameters from tracer temporal moments, (3) Evaluating the effects of correlations between S_N and K on tracer transport, and

how these correlations affect our ability to estimate NAPL spatial distribution parameters, and (4) Examining relationships between local parameters, such as K and S_N, and trajectory-integrated parameters, such as tracer travel time t and trajectory-average NAPL content, $\hat{S}$. The effects of nonlinear and nonequilibrium partitioning, effects that in addition to correlations between S_N and K, may confound the excess spreading approach, were evaluated in laboratory experiments, described in a separate section below. Determining relationships between local and trajectory-integrated parameters is important because field methods such as soil coring provide local or point information about K and S_N, while tracer tests provide solute trajectory integrative information.

[29] A suite of simulations was conducted using a range of hydraulic conductivity field variances and NAPL spatial distributions. Solute transport was modeled using a particle tracking approach described below. Breakthrough curves were generated from particle arrival times and temporal moments were determined by numerical integration. The NAPL spatial distribution parameters f, $\mu_{\ln \hat{S}}$, $\sigma_{\ln \hat{S}}$ and $\rho_{t,\hat{S}}$ were estimated using the measured moments and the distributed binary model equations, (19)–(21). The homogeneous and distributed models were compared using the laboratory experiments.

3.1. Particle Tracking Approach

[30] Tracer transport through heterogeneous domains was modeled using the particle tracking methodology described by *Demmy* [1999]. A summary of the simulation methods follows; additional details are given by *Demmy* [1999] and *Demmy et al.* [1999]. A turning bands algorithm [*Tompson et al.*, 1989] was used to generate a flow domain of 82 × 40 × 40 grid blocks with an exponentially correlated, lognormally distributed, isotropic saturated hydraulic conductivity field with $\mu_{\ln K} = 0.0$ and a correlation length, λ, of 8 grid blocks. A series of simulations was conducted with log conductivity field variances $\sigma^2_{\ln K} = \{0.05, 0.2, 1.0, 2.0, 4.0, 6.0\}$. The $\sigma^2_{\ln K} = \{0.2, 1.0\}$ simulations were used to evaluate the distributed binary model, while the entire suite of simulations was used to explore relationships between the statistics of local parameters ($\sigma^2_{\ln K}$ and $\sigma^2_{\ln S}$) and trajectory-integrated parameters ($\sigma^2_{\ln t,np}$ and $\sigma^2_{\ln \hat{S}}$), and to investigate the effects of correlations between S_N and K on these relationships.

[31] Constant head boundaries were specified at $x = 0$ and $x = 82$ with an average gradient of 0.01 and a homogeneous mobile water content of 0.2. A mixed finite element scheme was used to generate a system of coupled pressure-velocity equations that were solved to produce a velocity field for input into a particle tracking scheme. A Monte Carlo approach, similar to that suggested by *Cvetkovic et al.* [1998], was employed wherein $n = 5000$ realizations of the flow field were generated and a single particle was injected into each at $x = 1$, $y = 20$, $z = 20$. Particle arrival times and travel lengths were recorded at the $x = 81$ control plane, resulting in a nominal travel distance of 10 λ. This multirealization approach results in a collection of n statistically independent trajectories with a uniform resident injection boundary condition [*Demmy et al.*, 1999]. However, flux-weighted injection is more representative of interwell tracer tests, and the measured arrival times were thus weighted by their initial velocities, v_0 (see *Kreft and Zuber* [1978] and *Demmy et al.* [1999] for discussions on the significance of uniform versus flux boundary conditions).

[32] Solute BTCs are analogous to PDFs, but because of the discrete nature of the particle tracking method, particle arrival time distributions were represented as cumulative distribution functions (CDFs), $P(t)$. The arrival times were ranked in ascending order of their numerical values and, because each time was weighted by its instantaneous velocity at the time of injection, flux-weighted CDFs were generated from the ordered nonpartitioning and partitioning particle arrival times as follows:

$$P(t_i) = \frac{\sum_{j=1}^{i} v_{0,j}}{\sum_{j=1}^{n} v_{0,j}} \tag{26}$$

where $P(t_i)$ represents the probability that the arrival time of particle i is less than or equal to t.

3.2. Correlation Between S_N and K

[33] Many investigators have studied the effects of a correlation between hydraulic conductivity, or media permeability, and sorption coefficient, K_d, on solute transport through the use of numerical or analytical models [*Valocchi*, 1989; *Cvetkovic and Shapiro*, 1990; *Robin et al.*, 1991; *Bellin et al.*, 1993; *Tompson*, 1993]. All of these studies have shown that a negative correlation between K_d and K leads to enhanced spreading relative to the uncorrelated case, while a positive correlation leads to less spreading. For the negatively correlated case, reactive tracers traveling along low velocity (i.e., low permeability) streamlines will experience high K_d values and be more retarded, leading to longer travel times and more-elongated BTCs. For the positively correlated case, reactive solutes traveling along high velocity streamlines will be more highly retarded, allowing the solutes traveling along the low velocity, and low retardation, streamlines to catch up, resulting in more-compressed BTCs.

[34] Similar effects would be expected for correlations between S_N and K; however, little experimental evidence exists to support a general model for a correlation between these parameters. Also, because media properties and model parameters are often inferred from tracer arrival time distributions, as will be done here, any correlation between the local parameters S_N and K may be of secondary importance to correlations between the trajectory-integrated parameters $\hat{S}_N$ and t_{np}. In many scenarios, the solute arrival time for a given streamline can be considered to be inversely proportional to K. Correlations between S_N and K can then be transformed to correlations between S_N and t. However, for three-dimensional heterogeneous fields, solute path lengths are not likely to be equal for each streamline. Also, for domains that are more complex than simple linear flow systems, solute travel time may be affected by factors other than hydraulic conductivity. In doublet well patterns, for example, a wide distribution of streamline lengths is produced by the flow system geometry even in homogeneous media, and solute travel times and K are not directly proportional. Therefore, any correlations that may exist between S_N and K may be only weakly manifested in measured BTCs.

[35] However, for comparison with the extensive literature on the correlation between K_d and K, correlations between S_N and K were included in the numerical simulations presented below and the effect of these correlations on $\hat{S}_N$ and t_{np} is discussed. It will be assumed here that the general framework that has been developed for investigating correlations between K_d and K is applicable for S_N and K, subject to the consideration of constraints specific to NAPL contamination. Field measurements have indicated an approximately linear relationship between the logarithms of K_d and K [*Robin et al.*, 1991; *Tompson*, 1993]. By substituting $S = S_N/(1 - S_N)$ for K_d and adding an uncorrelated component, W, this relationship can be expressed as follows:

$$\ln S = \ln a + b \ln K + c \ln W \tag{27}$$

where W is a lognormally distributed random variable ($\mu_{\ln W} = 0$, $\sigma_{\ln W} = \sigma_{\ln K}$) with the same spatial correlation structure as the K field, but uncorrelated to log conductivity. Note that as with $\hat{S}$ and $\hat{S}_N$ above, S, not S_N, is assumed to be lognormally distributed and correlated to K; however, for low NAPL saturations, S approaches S_N.

[36] A relation similar to (27) was employed by *Cvetkovic et al.* [1998]. For $b \neq 0$, S and K approach perfect correlation (i.e., $\rho_{S,K} = \pm 1$) as $c \rightarrow 0$, while $b = 0$ results in the uncorrelated case. A simplified approach is to assume $\ln a = c = 0$ and investigate the effects of perfect positive and negative correlation, with $b > 0$ and $b < 0$, respectively. Modeling and analytical studies often implement this approach with $b = \pm 1$ [e.g., *Bellin et al.*, 1993; *Bosma et al.*, 1993; *Soerens et al.*, 1998]. However, the resulting variability in S or K_d will be equivalent to the K variability and may be unrealistically high. *Tompson* [1993] selected values of $\ln a$ and b to more closely mimic field measurements, but only investigated perfect correlation (i.e., $c = 0$).

[37] For each $\sigma^2_{\ln K}$, separate particle tracking simulations were conducted assuming zero, positive, and negative correlations between S and K. Based on the arguments presented above, a relatively large value of $c = 0.75$ was selected here to create a weak correlation between S and K, and values of $b = \pm 0.3$ were selected to restrict the S values to a more limited range than K. Note that by rewriting (27) as $S = aK^bW^c$, it is apparent from (16) that $\mu_{\ln S} = \ln a$ and $\sigma_{\ln S} = (b^2\sigma^2_{\ln K} + c^2\sigma^2_{\ln W})^{0.5}$. For each flow field, the average NAPL saturation was set to $\bar{S}_N = 0.05$ using $a = \{0.052, 0.049, 0.038, 0.027, 0.014, 0.007\}$ for increasing values of $\sigma^2_{\ln K}$, respectively. For the uncorrelated cases, $c = 0.808$ was selected to maintain the same S distribution mean and variance as the correlated cases.

3.3. Streamtube Average NAPL Saturation

[38] The average value of S that was observed along the trajectory of each particle was calculated as follows:

$$\hat{S} = \frac{\int_0^L \frac{S(x)dx}{v(x)}}{\int_0^L \frac{dx}{v(x)}} \tag{28}$$

where the inverse velocity integrated over trajectory length L is the travel time. The resulting trajectory-mean $\hat{S}$ values are analogous to the Lagrangian reaction flow path parameter, M, described by *Cvetkovic et al.* [1998]. It is emphasized that it is the $\hat{S}$ distribution for which statistics may be determined from (19)–(21).

[39] The simulations for log conductivity variance $\sigma^2_{\ln K} = \{0.2, 1.0\}$ were conducted with $f = \{0.1, 0.4, 0.6, 1.0\}$ and $\{0.25, 0.5, 0.75, 1.0\}$, respectively. For a randomly selected fraction $(1\text{-}f)$ of the particle trajectories, $K_N = 0$ was imposed so that the nonpartitioning and partitioning tracer arrival times would be equal. For the remaining particle trajectories (i.e., the contaminated fraction), $t_{p,c}$ was determined from the nonpartitioning tracer arrival time as described in (15) with $K_N = 20$.

[40] The $\hat{S}$ values determined from (28) were weighted by $v_{0,i}$ in order to represent a flux-averaged injection condition. The measured statistics of this distribution were compared to the estimates determined from the tracer temporal moments and (19)–(21).

3.4. Simulation Results

3.4.1. Nonpartitioning Tracer Transport

[41] The nonpartitioning tracer travel time distribution measured from each flow field was well described by a lognormal distribution. The lognormal model parameters $\mu_{\ln t,np}$ and $\sigma_{\ln t,np}$ were determined for each flow field from the nonpartitioning tracer normalized first and second temporal moments using (22) and (23). The flux-weighted measured nonpartitioning tracer CDF for $\sigma^2_{\ln K} = 1$ is shown in Figure 2 with the corresponding fit of (1) (partitioning tracer CDFs, discussed below, are also shown in Figure 2). Nonpartitioning tracer CDFs for the other $\sigma^2_{\ln K}$ values tested here were equally well represented by lognormal distributions (not shown).

[42] The parameters $\mu_{\ln t,np}$ and $\sigma^2_{\ln t,np}$ that were estimated for each flow field are shown in Figure 3 as a function $\sigma^2_{\ln K}$. A linear relationship was observed between $\sigma^2_{\ln K}$ and $\sigma^2_{\ln t,np}$, with a slope of 0.16, indicating that much of the variability in the point statistics was damped out in the integrated measure and the degree of dampening did not change as system variability increased. Similar effects were also reflected in the $\hat{S}$ distribution statistics, discussed below. Also note that $\mu_{\ln t,np}$ decreased as $\sigma^2_{\ln K}$ increased, with a slope of -0.21, indicating that the Lagrangian velocity through the flow field increased with $\sigma^2_{\ln K}$. This result is consistent with Lagrangian stochastic theory [e.g., *Demmy*, 1999].

3.4.2. Partitioning Tracer Transport

[43] Measured partitioning tracer CDFs are shown in Figure 2 for zero, positive, and negative correlation between K and S for $\sigma^2_{\ln K} = 1$ with contaminated fractions $f = \{0.25, 0.75, 1.0\}$. The CDFs from the other flow fields showed similar trends. Model parameters were determined from the nonpartitioning and partitioning tracer moments, and model CDFs were generated from the superposition of solutions of (1) for the uncontaminated and contaminated zones, as discussed above. The model fits matched the measured CDFs closely.

[44] Positive correlation between K and S ($b > 0$) led to greater partitioning tracer retardation than for the uncorrelated case, while negative correlation led to less retardation. Similar effects with K and K_d correlations have been

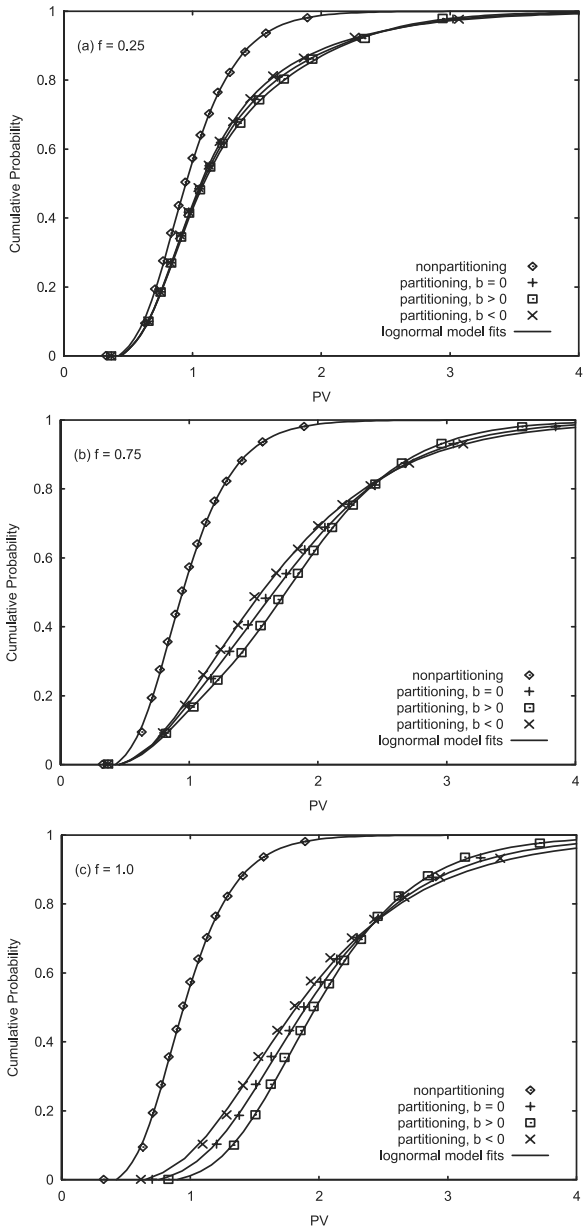

Figure 2. Nonpartitioning and partitioning tracer CDFs from particle tracking simulations with $\sigma^2_{\ln K} = 1.0$. Simulation results (points) are compared with model fits (lines) determined from CDF moments and (19)–(21) (i.e., distributed binary model) for (a) $f = 0.25$, (b) $f = 0.75$, and (c) $f = 1.0$.

observed in numerical simulations by *Tompson* [1993] and predicted theoretically by several investigators [*Dagan*, 1989; *Kabala and Sposito*, 1991; *Cvetkovic et al.*, 1998]. These effects increased as log conductivity variance increased (Figure 4), with approximately symmetric magnitudes for positive and negative correlations. Note that the coupled effects of media heterogeneity and positive correlations between K and S may result in overpredictions of the amount of NAPL present in a system, while negative correlations may result in underpredictions.

[45] Also, partitioning tracer CDFs for $b < 0$ exhibited enhanced spreading compared to $b = 0$, while $b > 0$ led to reduced spreading (Figure 2). This effect has also been

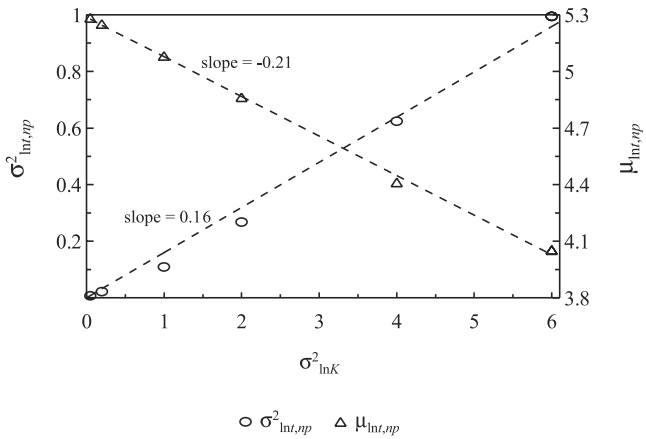

Figure 3. Nonpartitioning travel time lognormal model parameters, $\sigma^2_{\ln t,np}$ and $\mu_{\ln t,np}$, as a function of log conductivity variance, $\sigma^2_{\ln K}$. Dashed lines are linear regressions.

either predicted or observed by several investigators [*Kabala and Sposito*, 1991; *Bellin et al.*, 1993; *Bosma et al.*, 1993; *Tompson*, 1993]. Correlation effects on tracer CDF spreading, quantified by the second central moment ($\mu'_{2,p} = m_2 - m_1^2$), were also enhanced as log conductivity variance increased (Figure 5).

3.4.3. NAPL Saturation Distribution

[46] The actual and estimated model parameters that describe the NAPL saturation distribution are compared in Figure 6 and Table 1. For all values of f, $\sigma^2_{\ln K}$, and b that were evaluated, the estimated values of f matched the measured values closely (Figure 6). The $\hat{S}$ distribution model parameters ($\mu_{\ln \hat{S}}$, $\sigma_{\ln \hat{S}}$, and $\rho_{t,\hat{S}}$) estimated from (19)–(21) also compared favorably with the measured values (Table 1). The reported values are the mean and standard deviation from the four f values tested for each combination of $\sigma^2_{\ln K}$ and b. The RMSD between the measured and model fit

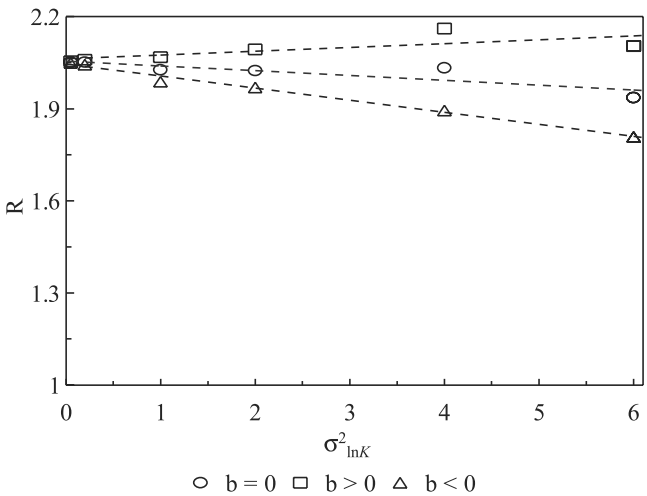

Figure 4. Partitioning tracer retardation, R, as a function of log conductivity variance $\sigma^2_{\ln K}$ for zero, positive, and negative correlation between K and S. Dashed lines are linear regressions.

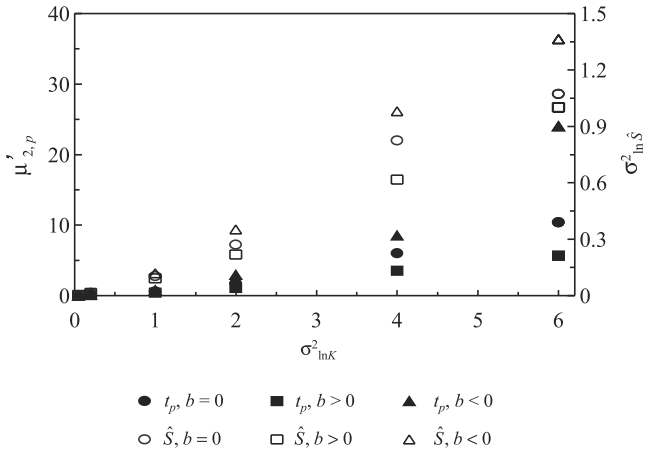

Figure 5. Second central moment, $\mu'_{2,p}$, for partitioning tracer travel time t_p and variance of trajectory-average NAPL saturation $\sigma^2_{\ln\hat{S}}$ as a function of log conductivity variance $\sigma^2_{\ln K}$ for zero, positive, and negative correlation between K and S.

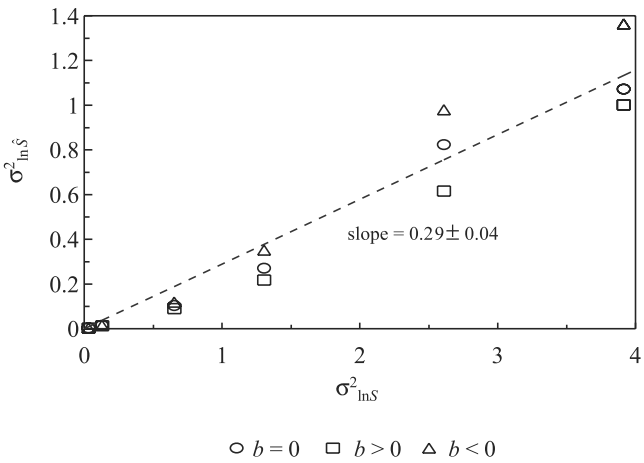

Figure 7. Relationship between variances of trajectory-average and local NAPL contents, $\sigma^2_{\ln\hat{S}}$ and $\sigma^2_{\ln S}$, for zero, positive, and negative correlation between K and S. Dashed line is a linear regression.

partitioning tracer first three normalized temporal moments is also reported. The correlation between the nonpartitioning tracer travel time and $\hat{S}$, $\rho_{t,\hat{S}}$, was calculated using (17). Note that, because of the inverse relationship between K and t, a positive correlation between K and S resulted in a negative value of $\rho_{t,\hat{S}}$, and vice versa.

[47] As was observed with K and t_{np}, much of the point variability in S was damped out in the trajectory-integrated measure, $\hat{S}$. A linear relationship was observed between $\sigma^2_{\ln S}$ and $\sigma^2_{\ln\hat{S}}$, with a slope of 0.29 ± 0.04 (mean and standard deviation for the three correlation cases, Figure 7), again indicating that the degree of dampening did not change with system variability. The measured correlations between t_{np} and $\hat{S}$ were also affected by system heterogeneity. The absolute values of $\rho_{t,\hat{S}}$ decreased linearly with $\sigma^2_{\ln K}$, with symmetric slope absolute values of 0.04 for both correlated cases (Figure 8). Note, however, that while $\rho_{t,\hat{S}}$ decreased with $\sigma^2_{\ln K}$, the relative effects of a correlation between K and S on reactive tracer travel time mean and variance increased with log conductivity variance (Figures 5 and 7).

[48] The errors associated with ignoring the correlation between K and S were also investigated. The estimated $\hat{S}$ distribution parameters that resulted when the constraint $\rho_{t,\hat{S}} = 0$ was imposed for $\sigma_{\ln K}{}^2 = 0.2$ and $b < 0$ are listed in Table 1. Note that very good agreement was obtained with the measured partitioning tracer moments (as reflected in the RMSD) and $\mu_{\ln\hat{S}}$, but the $\sigma_{\ln\hat{S}}$ estimates were relatively poor (as were, of course, the $\rho_{t,\hat{S}}$ estimates). These results point to the potential pitfall, when using tracer BTC moments for parameter estimation, of multiple solutions producing moment estimates that are quite close to the measured values. In this example, assuming $\rho_{t,\hat{S}} = 0$ allowed algebraic solution of (19)–(21) and, thus, a low RMSD. While the more-correct solutions (i.e., $\rho_{t,\hat{S}} \neq 0$) produced lower RMSD values here (Table 1), it may be difficult to

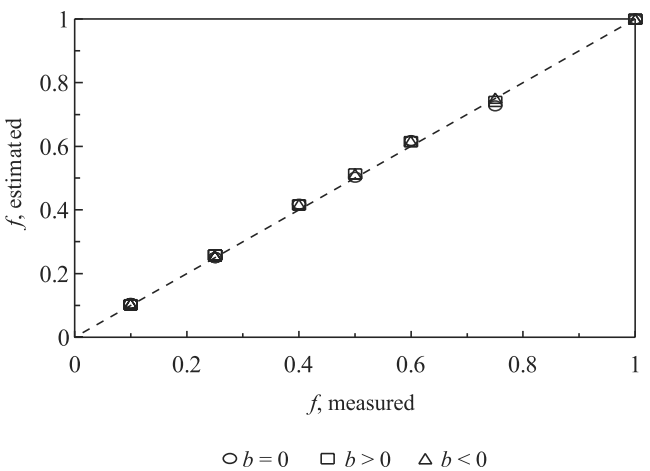

Figure 6. Measured and estimated values for contaminated fraction f for zero, positive, and negative correlation between K and S. Results for f = {0.1, 0.4, 0.6, 1.0} and {0.25, 0.5, 0.75, 1.0} are from simulations with $\sigma^2_{\ln K} = 0.2$ and 1.0, respectively. Dashed line is 1:1 relationship.

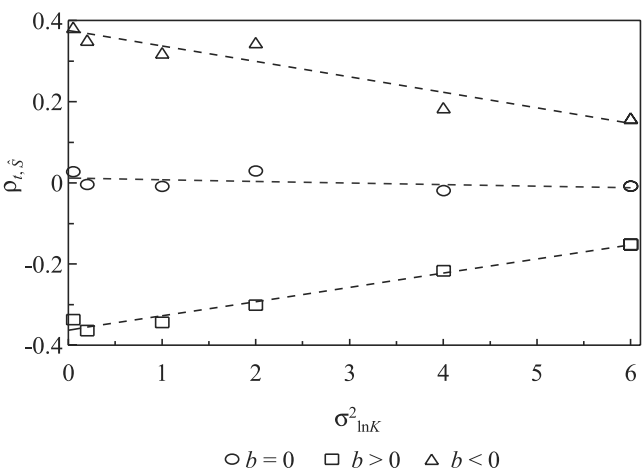

Figure 8. Measured correlation between partitioning tracer travel time and trajectory-average NAPL saturation as a function of $\sigma^2_{\ln K}$ for zero, positive, and negative correlation between K and S. Dashed lines are linear regressions.

differentiate between the solutions for $\rho_{t,\hat{S}} = 0$ and $\rho_{t,\hat{S}} \neq 0$ with no prior information as to the expected correlation between K and S. However, while the $\hat{S}$ distribution parameters $\rho_{t,\hat{S}}$ and $\sigma_{\ln \hat{S}}$ for this case did not accurately reflect the true distribution, the estimated f values were nearly identical to the 'more-correct' model fit values shown in Figure 6 (the average relative difference was 0.13%). This result suggests that for moderate correlations between K and S, reasonable estimates of the fraction of the streamtubes in the domain that are contaminated may be obtained even if correlation effects are ignored.

[49] Finally, it is noted that the effects on the retardation and spreading of the partitioning tracer CDFs that resulted from correlations between K and S were manifestations of the effects of these correlations on the $\hat{S}$ distribution. A positive correlation between K and S resulted in increased $\mu_{\ln \hat{S}}$ and decreased $\sigma_{\ln \hat{S}}$ values, with reverse relationships for negative correlation (Table 1). The linkage between the spreading of the $\hat{S}$ and t_p distributions is illustrated in Figure 5, where $\sigma^2_{\ln \hat{S}}$ and $\mu'_{2,p}$ are shown as functions of $\sigma^2_{\ln K}$.

3.5. Summary of Simulation Results

[50] The particle tracking simulations indicated that (1) Local (point) parameter variability (quantified by $\sigma^2_{\ln K}$ and $\sigma^2_{\ln S}$) was linearly damped in the statistics of trajectory-averaged parameters ($\sigma^2_{\ln t,np}$ and $\sigma^2_{\ln \hat{S}}$), (2) Reactive tracer retardation and spreading increased with increasing hydraulic conductivity variance, and with negative correlation with NAPL content, and (3) The distributed binary model enabled accurate estimation of NAPL spatial distribution parameters for a range of hydraulic conductivity variances with correlations between K and S. The observed relationships between local and integrated parameters may be useful for empirically relating tracer test results to point measurements, or for comparison with theoretical relationships between point and integrated statistics such as those that may be developed in the stochastic Lagrangian framework [e.g., *Cvetkovic et al.*, 1998; *Demmy et al.*, 1999].

4. Laboratory Studies

[51] Laboratory experiments were conducted in a flow chamber that was packed with various combinations of clean 20–30 mesh Ottawa sand and sand mixed with *n*-decane, resulting in a range of contaminated fractions $f = \{0.16, 0.29, 0.38, 0.48, 0.57\}$. Partitioning tracer tests were conducted for each combination, and nonpartitioning and partitioning tracer BTC moments were calculated with the goal of recovering the design parameters f and $\bar{S}_N$ using the homogeneous and distributed binary models. The relative impacts of nonlinear and nonequilibrium partitioning on the estimation of these parameters were also investigated.

4.1. Nonequilibrium and Nonlinear Partitioning

[52] *Valocchi* [1985] described the effects of nonequilibrium sorption, or partitioning, on solute BTCs and ADE temporal moments, demonstrating that nonequilibrium effects lead to enhanced spreading (i.e., larger second and third moments) relative to equilibrium conditions. *Jin et al.* [1995] found that pore water velocities of 0.5 to 1.5 m/d were slow enough to approximate equilibrium conditions for partitioning of alcohol tracers into tetrachloroethylene. The models developed here are based on the assumption that partitioning tracer residence times are sufficient to ensure equilibrium partitioning. However, the velocities suggested by *Jin et al.* [1995] are quite low and may be impractical for field-scale experiments. In addition, *Willson et al.* [2000] observed nonequilibrium partitioning effects in laboratory-scale tracer tests conducted at higher velocities. Thus, the impact of using higher velocities was investigated in the laboratory experiments reported below.

[53] While the partitioning of alcohol tracers into NAPLs has been demonstrated to be nonlinear [*Wise et al.*, 1999], which may lead to significant errors in $\bar{S}_N$ estimates if partitioning is assumed to be linear [*Wise*, 1999], the common practice of using a suite of partitioning tracers [e.g., *Jin et al.*, 1995; *Annable et al.*, 1998] has been shown to cause partitioning behavior to approach linearity [*Wise*, 1999]. Thus, for this work, wherein at least two partitioning tracers were always used in concert, linear partitioning was assumed. Also, *Wise* [1999] suggested that consideration of isotherm linearity should be made during tracer selection and that nonlinear effects can be minimized by using low tracer injection concentrations. The effect of varying tracer injection concentrations, and thus, the degree of nonlinearity, was investigated in the laboratory experiments described below.

4.2. Laboratory Experimental Methods

[54] The laboratory flow chamber was similar in design to that described by *Jawitz et al.* [1998a]. The open-top chamber enclosed a volume of 62 cm length, 1.4 cm width, and 39 cm height and was constructed of two glass plates closed on three sides by 1.3 cm square aluminum tubing. The vertical sections of tubing on either end were slotted to a width of 0.03 cm at a frequency of 4 slots per cm, enabling homogeneous injection and extraction of fluids. Clean zones were packed by slowly pouring untreated sand into standing water in the chamber, while contaminated zones were created by adding premixed sand, water, and *n*-decane in approximately 10-g increments. Decane was selected as the NAPL because of its low aqueous solubility (0.009 mg/L [*Verschueren*, 1983]), facilitating multiple tracer tests without significant NAPL mass loss due to dissolution. The water table was maintained at the top of the media during the addition of contaminated sand to minimize gravity segregation of the sand, water, and decane during emplacement.

[55] In the initial experiment, labeled configuration 1 (C1, Table 2), 5.4 mL of *n*-decane were thoroughly mixed with 731 g of clean sand and emplaced in a 5 cm high contaminated layer wherein the NAPL was assumed to be homogeneously distributed. An additional 548 g of clean sand were added, resulting in a total packed height of 8.5 cm, total pore volume (PV) of 270 mL, and $\bar{S}_N = 0.020$. The resulting contaminated fraction $f = 0.57$ was based on the total masses of clean and contaminated sand that were packed; however, the effective volumetric fraction may have varied from the mass-based value because of nonuniform packing or trapped air.

[56] For C2, the flow chamber was repacked with 7.5 mL of *n*-decane (more NAPL was added to increase partitioning tracer retardation) in a 5 cm layer with an additional 797 g of clean sand, resulting in $f = 0.48$ and $\bar{S}_N = 0.023$. For subsequent configurations, the contaminated fraction was

Table 2. Laboratory Experimental Configurations, Including Pore Water Velocities, Partitioning Tracer Initial Concentrations, Pore Volume (PV), Domain-Average NAPL Saturation, and Contaminated Fraction for Each Experiment[a]

Experiment Number	v, m/d	DMP, mg/L	6M2H, mg/L	Height, cm	Clean Sand, g	PV, mL	$\bar{S}_N$	f
Configuration 1	11	300	300	8.85	548	270	0.020	0.57
Configuration 2				10.4	797	317	0.022	0.48
C2-1 (v_0, C_0)	17	500	180					
C2-2 ($v_0/2$, C_0)	8.7	500	180					
C2-3 ($v_0/6$, $0.5C_0$)	2.9	250	90					
C2-4 ($v_0/6$, C_0)	2.9	500	180					
C2-5 ($v_0/6$, $2C_0$)	2.9	1000	360					
C2-6 ($v_0/6$, $3C_0$)	2.9	1500	540					
C2-7 ($v_0/12$, C_0)	1.4	500	180					
Configuration 3	8.9	1500	540	13.0	1197	421	0.018	0.38
Configuration 4	9.4	1500	540	16.7	1797	553	0.014	0.29
Configuration 5	10	1500	540	29.0	3827	954	0.008	0.16

[a]Methanol initial concentrations were 2500 mg/L for all experiments except C1 (2000 mg/L). The mass of sand in the contaminated zone was 731 g for each experiment. Note that partitioning tracer C_0 values were equivalent to approximately 6% of aqueous solubility.

sequentially reduced by adding clean sand to the top of the packing. The total packed height and the total mass of clean and contaminated sand in each packing are listed in Table 2. The mean and standard deviation bulk density of the five packing configurations was 1.76 ± 0.05 g/cm^3, which, assuming a sand grain density of 2.65 g/cm^3, corresponds to porosity $\eta = 0.34 \pm 0.02$.

[57] A constant head reservoir was used to deliver fluids to the flow chamber through the injection well, and a positive displacement pump (Masterflex L/S drive equipped with a Fluid Metering Inc. Q Pump head) was used to remove fluids through the extraction well. The effluent was pumped through an in-line flow cell attached to a gas chromatograph equipped with an autosampler (Perkin Elmer AutoSystem), allowing quantification of tracer concentrations without manual sampling [*Jawitz et al.*, 2002]. For each partitioning tracer test, a tracer pulse of approximately 0.15 PVs was delivered to the injection well with a syringe pump (Harvard Apparatus 22) during steady-state water flow. During each tracer test, wax paper was placed over the media-air interface to minimize volatile losses of tracers. Experiments were continued until tracer concentrations measured in the effluent were below detection limit (generally 1 mg/L). The measured BTCs were relatively complete, but exponential extrapolation [*Sater and Levenspiel*, 1966] was employed to improve moment estimate accuracy.

[58] Methanol was used as the nonpartitioning tracer, with 2,2-dimethyl-3-pentanol (DMP) and 6-methyl-2-heptanol (6M2H) as partitioning tracers. The fluid flow rates and tracer initial concentrations were varied for C2 (Table 2) to investigate the effects of nonequilibrium and nonlinear partitioning, respectively. Average pore water velocities and tracer injection concentrations for each of these experiments are also listed in Table 2.

[59] The velocity of experiment C2-1 was chosen as an upper limit of approximately 10 times that suggested by *Jin et al.* [1995] for equilibrium conditions. Velocities lower than 1.4 m/d (C2-7) were not investigated because of concerns about mass loss of tracers due to volatilization. Also, field experimental experience suggests that lower velocities may not be practical for field implementation [*Annable et al.*, 1998; *Jawitz et al.*, 1998c, 2000].

[60] The aqueous solubility of DMP has been reported to be 8200 mg/L [*Barton*, 1984] and the solubility of 6M2H was estimated to be approximately 3000 mg/L (based on the solubilities of other methylated heptanols, as reported by *Barton* [1984]). The relatively low C_o values for DMP and 6M2H in C2-1 (approximately 6% of aqueous solubility) were selected to minimize the effects of NAPL-water tracer partitioning isotherm nonlinearities, demonstrated by *Wise* [1999] to become significant at C_o values above approximately 10% of aqueous solubility. In subsequent experiments, these C_o values were varied to ascertain whether nonlinear partitioning was a factor in these experiments. Decane-water partitioning coefficients for DMP and 6M2H, K_N = 12 and 25, respectively, were measured using batch equilibration methods.

4.3. Laboratory Results

4.3.1. Nonlinear and Nonequilibrium Partitioning

[61] The measured partitioning tracer BTCs from C2-1–C2-7 are shown in Figures 9a (C2-3–C2-6) and 9b (C2-7, C2-4, C2-2, and C2-1), where each BTC was scaled to its zeroth moment (note that relative concentration, C/C_0, is plotted on log scale). The partitioning tracer BTCs were bimodal, with the first and second modes reflecting transport through the uncontaminated zone and contaminated zones, respectively, as expected for a homogeneous binary NAPL distribution [*Jawitz et al.*, 1998b]. The nonpartitioning tracer behavior was very similar for each experiment, indicating consistent hydrodynamics (these BTCs were omitted from Figure 9 to more clearly reveal the partitioning tracer behavior), with $\mu_{\ln t,np} = 0.059 \pm 0.003$ and $\sigma_{\ln t,np} = 0.119 \pm 0.015$ for C2-1–C2-7 (determined from tracer normalized temporal moments, units of PV^N, using (22) and (23)).

[62] The tracer transport behavior in C2-3, C2-4, C2-5, and C2-6 (Figure 9a) was very similar, despite the fact that these experiments were conducted with tracer C_0 values ranging from approximately 3 to 18% of aqueous solubility. *Wise* [1999] demonstrated that the effects of isotherm nonlinearities would be expected to increase with C_0. The results presented here, therefore, indicate that partitioning isotherm nonlinearities were not a significant concern in these experiments. However, the BTCs presented in Figure 9b, which are from experiments conducted at four different pore water velocities, show increased spreading in the second mode as pore water velocity increased, as would as would be expected for rate-limited sorption, or partitioning [e.g., *Valocchi*, 1985]. Thus, these results indicate that nonequilibrium partitioning likely was a factor in these experiments.

[63] In some low-velocity experiments, it was observed that the spreading of the first mode of the partitioning tracer BTCs was greater than that of the nonpartitioning methanol BTC. It is likely that at very low velocities tracer diffusion between the contaminated and uncontaminated zones is not negligible. Therefore, subsequent experiments were conducted at intermediate velocities, despite possible partitioning rate limitations.

4.3.2. Estimation of f and $\bar{S}_N$

[64] The first three normalized temporal moments determined from the nonpartitioning and partitioning tracer BTCs

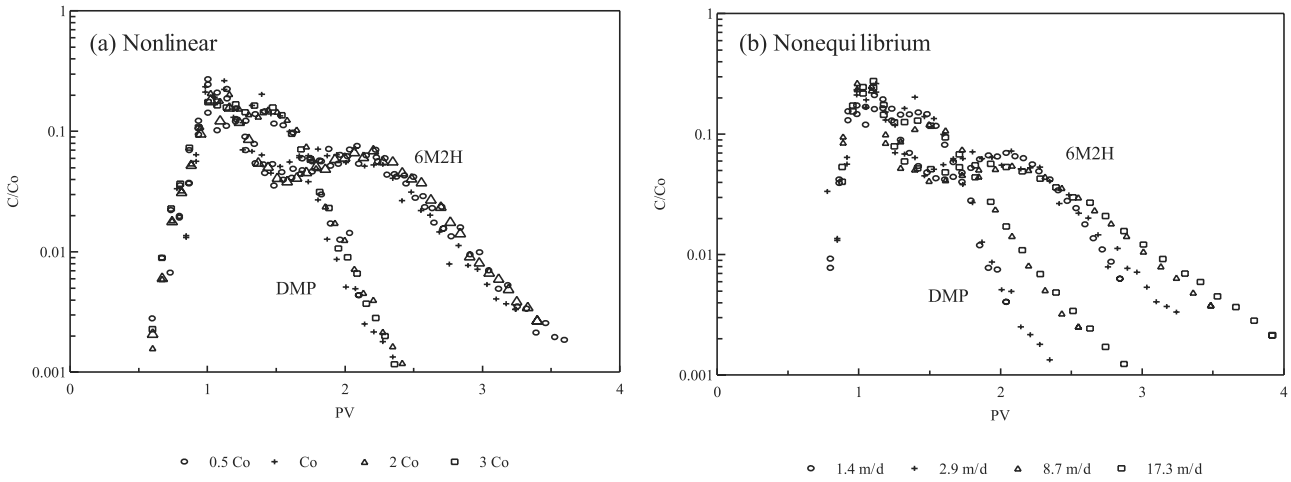

Figure 9. Partitioning tracer BTCs from experiments with (a) equivalent velocities v = 2.9 m/d, but varying initial concentrations (C2-3, C2-4, C2-5, and C2-6), and (b) equivalent initial concentrations, approximately 6% of aqueous solubility, but varying velocities (C2-7, C2-4, C2-2, and C2-1).

are presented in Table 3. Results from C2-4 were selected to represent configuration 2. The domain-average NAPL saturation $\bar{S}_N$ was estimated for each configuration from both the DMP and 6M2H data using first moment analysis (i.e., using (4) and (5) after *Jin et al.* [1995]). The average relative difference between the actual and estimated $\bar{S}_N$ values from both tracers for all experiments was 0.02 ± 0.15.

[65] Parameters describing the NAPL saturation distribution were determined for each experimental configuration using both the homogeneous and distributed binary models (Table 3). The homogeneous binary model parameters were determined by algebraic solution of (13) and (14) using the first and second temporal moments of the measured tracer BTCs, while the distributed binary model parameters were determined by algebraic solution of (19)–(21) using the first, second, and third moments. For these experiments, $\rho_{t,\hat{S}} = 0$ was assumed. The model BTCs generated using the homogeneous and distributed model parameters are compared to the measured BTCs in Figures 10 and 11, respectively. Note that as f decreases, the proportion of a partitioning tracer BTC that results from transport through the contaminated zone decreases. Thus, the size of the second mode of the measured partitioning tracer BTCs decreases with f (Figure 10).

[66] The assumption of a uniform $\bar{S}_{N,c}$ limited the capability of the homogeneous model to capture the degree of spreading that was observed in the partitioning tracer BTC second modes (i.e., the contaminated zone portion) (Figure 10). Inclusion of the third moment and an additional model parameter (i.e., the variability of the $\hat{S}$ distribution) in the distributed model provided the flexibility to account for the observed excess spreading that may have resulted from either nonuniform NAPL distribution within the contaminated zone or rate-limited partitioning, and thus enhanced the goodness-of-fit of the model to the measured data compared to the homogeneous model (Figure 11). It is noted, however, that the f estimates were close to the true values for both models (Figure 12).

[67] Note that because of the ability of the distributed model to capture the observed excess spreading, the $\bar{S}_c$ values (reflected in $m_1^{\hat{S}}$) that were required to match the measured moments were lower than for the homogeneous model. Therefore, in order to maintain equal domain-average $\bar{S}_N$ values, the distributed model produced slightly higher f estimates than the homogeneous model (0.11 ± 0.06 relative difference for both tracers in all configurations). Thus, the two cases with the closest match between f estimates for the two models, f = {0.48 DMP, 0.16 DMP}, corresponded to the lowest values of $\sigma_{\ln \hat{S}}$ (i.e., the most homogeneous of the distributed model results), and resulted in the most similar fits to the measured data between the homogeneous and distributed models (DMP in Figures 10b and 11b and 10e and 11e).

5. Field Studies

[68] The distributed binary model was applied to data from field-scale partitioning tracer tests conducted at two NAPL-contaminated sites: Hill Air Force Base (AFB), UT and Jacksonville, FL. Detailed descriptions of these studies are given by *Jawitz et al.* [1998b, 2000], respectively.

5.1. Background and Methods

[69] The two field sites were contaminated with different types of NAPL, leading to different NAPL spatial distributions. The multicomponent NAPL at Hill AFB was less dense than water (LNAPL), while the primary contaminant at the Jacksonville site, tetrachloroethylene (PCE), was denser than water (DNAPL).

[70] Light NAPLs float on the water table, often creating smear zones as the water table fluctuates seasonally. At the Hill AFB site, the mean water table position was only approximately 1 m above a clay confining unit at 8 m below ground surface (bgs). Soil core data indicated a NAPL smear zone extending up from the clay to approximately 5 m bgs. The soil concentration profile for *n*-undecane, the most prevalent of the NAPL constituents at a mass fraction of 1.57g/100g, is presented in Figure 13; similar behavior was observed for the other NAPL constituents as well (data not shown). These data represent 85 subsamples from 8 borings

Table 3. Measured Nonpartitioning and Partitioning Tracer Moments (Units of PV^N) and Estimated NAPL Distribution Model Parameters for Each Laboratory Experiment[a]

	Measured Moments				Homogeneous Model		Distributed Model			
Tracer	m_1	m_2	m_3	$\bar{S}_N$	f	$\bar{S}_N$	f	$\mu_{\ln \hat{S}}$	$\sigma_{\ln \hat{S}}$	$\bar{S}_N$
C1										
Methanol	1.09	1.21	1.37							
DMP	1.29	1.73	2.45	0.016	0.51	0.016	0.56	−3.55	0.294	0.016
6M2H	1.49	2.46	4.51	0.016	0.45	0.016	0.53	−3.56	0.395	0.016
C2										
Methanol	1.07	1.15	1.27							
DMP	1.28	1.70	2.36	0.017	0.50	0.017	0.50	−3.35	0.106	0.017
6M2H	1.58	2.81	5.58	0.020	0.50	0.020	0.57	−3.38	0.376	0.020
C3										
Methanol	1.07	1.17	1.32							
DMP	1.27	1.72	2.54	0.016	0.34	0.016	0.40	−3.26	0.423	0.016
6M2H	1.61	3.04	6.75	0.021	0.43	0.021	0.48	−3.14	0.325	0.021
C4										
Methanol	1.07	1.17	1.33							
DMP	1.23	1.63	2.36	0.013	0.25	0.013	0.30	−3.16	0.411	0.013
6M2H	1.48	2.67	5.87	0.016	0.30	0.016	0.33	−3.01	0.294	0.016
C5										
Methanol	1.07	1.17	1.30							
DMP	1.17	1.47	2.10	0.008	0.12	0.008	0.12	−2.56	0.001	0.008
6M2H	1.31	2.14	4.56	0.010	0.15	0.010	0.16	−2.82	0.325	0.010

[a]Domain-average NAPL saturations, $\bar{S}_N$, were determined from measured first moments using equations (4) and (5), and from the distributed model parameters using equation (3) (with $m_1^{\hat{S}} = \bar{S}_c$) and $\bar{S}_N = f\bar{S}_c/(1+\bar{S}_c)$. Moment estimates obtained from both models were very close to the measured values (generally within 1%). Results from C2-4 were selected to represent configuration 2.

collected within the tracer swept volume during installation of wells and multilevel samplers.

[71] The Hill AFB experiments were conducted within a hydraulically isolated sheet pile test cell, enabling manipulation of the water table. During partitioning tracer tests, the water table in the test cell was maintained at approximately 5 m bgs (3 m above the clay) in order to capture the entire NAPL smear zone. Thus, it was expected that most of the streamlines within the test cell would intercept some NAPL ($f \rightarrow 1.0$).

[72] At the Jacksonville site, the areal and vertical extent of the NAPL source zone was less clear. Soil cores indicated

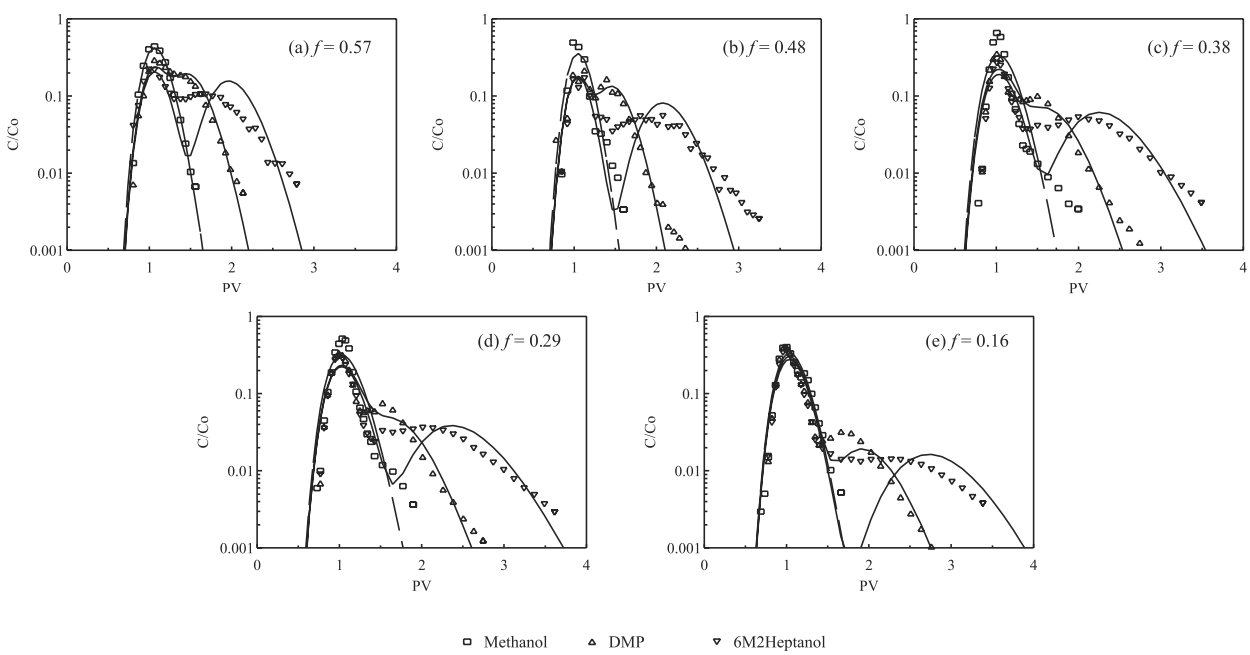

Figure 10. Measured nonpartitioning and partitioning tracer BTCs from (a) C1, (b) C2-4, (c) C3, (d) C4, and (e) C5, each shown with the homogeneous binary model fit.

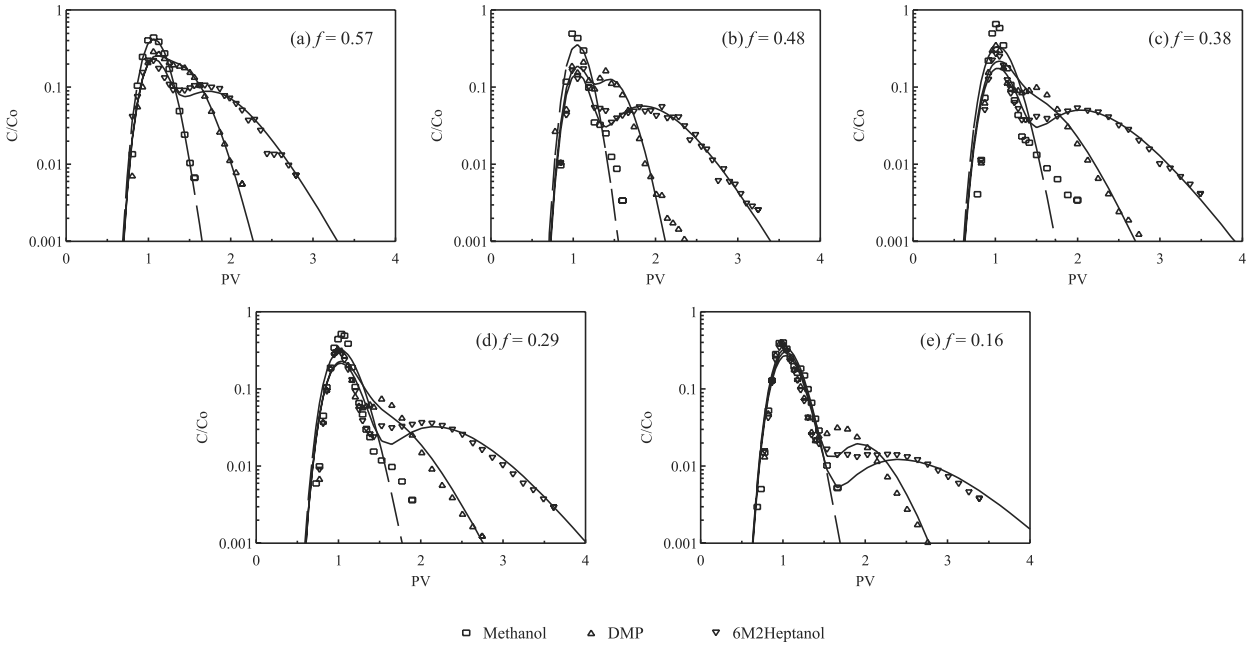

Figure 11. Measured nonpartitioning and partitioning tracer BTCs from (a) C1, (b) C2-4, (c) C3, (d) C4, and (e) C5, each shown with the distributed binary model fit.

a NAPL source zone between 7 and 10 m bgs that consisted of thin layers of separate phase PCE that were not necessarily horizontally continuous over the extent of the source zone. Example soil concentration profiles are presented in Figure 14. These data illustrate that much of the aquifer was uncontaminated. However, because of the likely presence of areally discontinuous NAPL layers located at different elevations throughout the source zone, the fraction of horizontal trajectories intercepting some amount of NAPL was likely greater than might be estimated from examination of individual borings.

[73] During tracer tests at the Jacksonville site, the DNAPL source zone was not physically bounded by sheet pile walls, the confining clay layer (located at approximately 11 m bgs), or the water table (approximately 3 m bgs), as at the Hill AFB site. Therefore, it was likely that some of the tracer solution followed streamlines through portions of the aquifer that were either above or below the NAPL source zone. Thus, while a precise *a priori* estimate of the fraction of the streamlines that might have intercepted some NAPL was not possible, it was estimated that a measurable fraction of the streamlines would be uncontaminated (i.e., $f < 1.0$).

[74] Methanol was used as the nonpartitioning tracer at both sites and the partitioning tracers were DMP ($K_N = 10.7$) and 2-ethyl-1-hexanol (e-HEX, $K_N = 81$) at the Hill AFB and Jacksonville sites, respectively. Both studies were conducted at flow rates that were equivalent to approximately 1 PV per day, with tracer input pulse durations $t_0 = 0.16$ and 0.20 PV for the Hill AFB and Jacksonville sites, respectively. The Hill AFB study was conducted in a line-drive pattern, with four injection wells and three extraction wells, with a mean pore water velocity of approximately 4 m/d. The results presented here are for the flux-average of the tracer BTCs measured at all three extraction wells. This approach represents information integrated over the entire test cell volume. The Jacksonville study was conducted with six recovery wells encircling three injection wells, with a mean velocity of approximately 7 m/d. The results presented here are from two recovery wells, labeled RWs 3 and 7, that represented the most DNAPL in their respective swept volumes, and the most reliable partitioning tracer results of all the recovery wells at the Jacksonville site (see *Jawitz et al.*'s [2000] Tables 1 and 2, respectively).

5.2. Moment Calculation and Model PDF Generation

[75] The BTCs from the laboratory experiments presented above were complete enough that simple exponential extrapolation provided adequate moment estimates; however, the BTCs from the field experiments were trun-

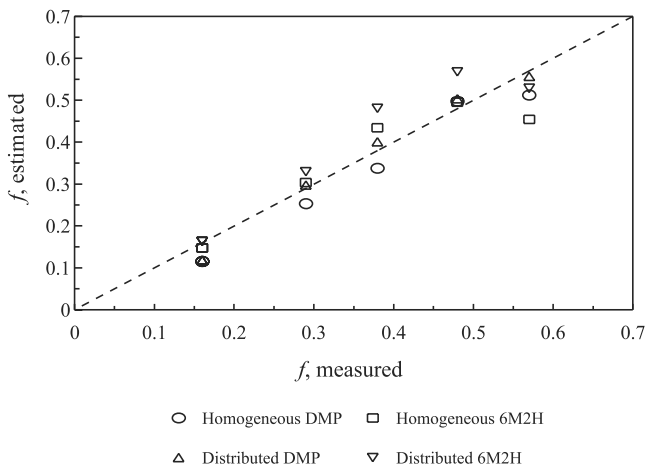

Figure 12. Measured and estimated values for contaminated fraction f from DMP and 6M2H BTC moments and the homogeneous and distributed binary models. Dashed line is 1:1 relationship.

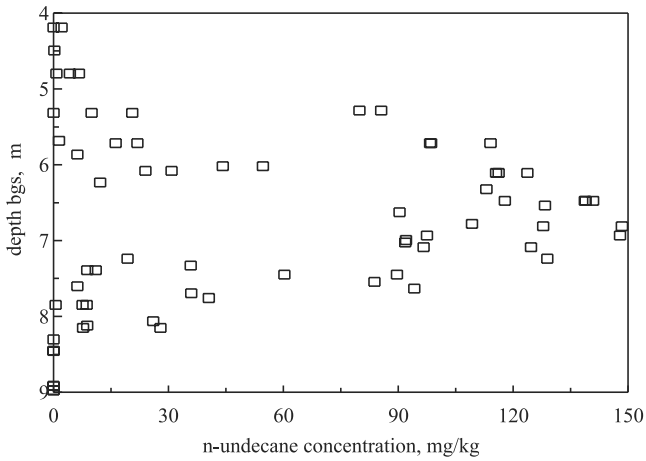

Figure 13. Soil concentration profile at Hill AFB, UT field site for *n*-undecane (determined from methylene chloride extracts of soil samples; n = 85 subsamples collected from eight borings). Water table position during tracer tests was maintained at approximately 5 m bgs (3 m above a clay layer found at 8 m bgs). Data were originally published by *Jawitz et al.* [1998c].

cated because of the dual limitations of analytical detection and experiment duration. *Helms* [1997] described a method for obtaining accurate estimates of complete moments from incomplete data by nonlinear regression of an appropriate model to the data. *Helms* [1997] found that the superposition of multiple ADE solutions performed well for fitting asymmetric BTCs characterized by an early peak followed by a long, dispersed tail typical of many field-measured BTCs. Following *Helms* [1997], the superposition of two lognormal distributions, similar to (25), was found to be sufficient to accurately fit the measured data:

$$p(t_{np}) = (1 - F)p_1(t) + Fp_2(t) \tag{29}$$

where $(1 - F)$ and F represent the fractional contributions of the lognormal PDFs $p_1(t)$ and $p_2(t)$. Complete moment estimates were then calculated for the incomplete BTC data using F and the parameters of $p_1(t)$ and $p_2(t)$ in a manner analogous to (10).

[76] While a sum of lognormal distributions may be approximated as lognormal, a superposition of lognormal distributions may not. That is, the sum of i lognormal distributions $Z = p_1 + p_2 + \cdots + p_i$ is lognormal [*Schwartz and Yeh*, 1982; *Abu-Dayya and Beaulieu*, 1994], but the superposition $Y = (1 - F)p_1 + Fp_2$, which may be bimodal, is not lognormal. Therefore, for cases where multimodal nonpartitioning tracer models are required, such as the field experiments reported here, t_{np} is not lognormal and $t_{p,c}$, therefore, may no longer be considered as a simple sum of lognormal distributions. In these cases, $t_{p,c}$ must be determined numerically by summing the CDFs of each term in (11) or (15). In the distributed binary model, for example, the CDF of the first term of (15), t_{np}, is determined by integrating the PDF determined from the superposition relation (29). The third term of (15) is a lognormal distribution multiplied by a constant and the CDF is generated by simply integrating the PDF. However, determination of the CDF for the second term of (15) requires multiplication of the CDFs for $\hat{S}$ and t_{np}. The model-predicted partitioning tracer BTC can then be determined by numerically differentiating the sum total CDF of (15). However, numerical differentiation may be subject to considerable errors (for a discussion of the potential pitfalls of numerical differentiation, see *Atkinson* [1985]). Therefore, the BTCs measured from the field experiments were numerically integrated such that comparisons were made between measured and modeled CDFs, rather than PDFs.

5.3. Field Results

[77] The first three temporal moments determined from measured nonpartitioning and partitioning tracer BTCs from both studies are presented in Table 4 (units are d^N). Tracer CDFs were determined by scaling the measured BTCs to their zeroth moments and integrating. Measured CDFs from the field studies are presented in Figures 15 and 16 along with the model fits for each. For both studies, the partitioning tracer CDFs that resulted from the application

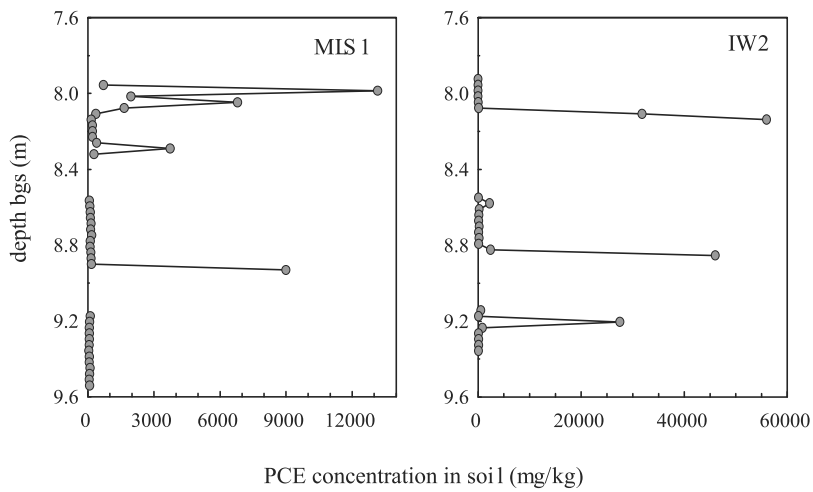

Figure 14. Soil concentration profiles at Jacksonville, FL, field site for PCE. Data are shown from two borings collected during installation of a multilevel sampler (MLS1) and an injection well (IW 2). Data were originally published by *Jawitz et al.* [2000].

Table 4. Nonpartitioning and Partitioning Tracer Moments (Units of d^N) and NAPL Saturation Distribution Parameters for the Hill AFB, Utah, and Jacksonville, Florida, Field Tracer Experiments[a]

	Moments				Model Parameters								
Tracer	m_1	m_2	m_3	$\bar{S}_N$	F	$\mu_{\ln t,1}$	$\sigma_{\ln t,1}$	$\mu_{\ln t,2}$	$\sigma_{\ln t,2}$	f	$\mu_{\ln \hat{S}}$	$\sigma_{\ln \hat{S}}$	$\bar{S}_N$
Nonpartitioning													
Hill AFB	1.23	2.93	16.0		0.19	−0.193	0.438	0.712	0.704				
Jax, RW 3	0.686	1.00	2.88		0.49	−1.24	0.390	−0.190	0.719				
Jax, RW 7	1.06	2.33	10.4		0.80	−0.865	0.193	−0.127	0.809				
Partitioning													
Hill - DMP	2.05	7.72	56.0	0.063						1.0	−2.81	0.029	0.057
Jax, RW 3 - EHex	0.864	1.71	6.48	0.003						0.69	−5.26	0.001	0.004
Jax, RW 7 - EHex	1.42	4.48	28.8	0.004						0.65	−4.98	0.001	0.004

[a]Model parameter subscripts 1 and 2 refer to the superposed lognormal distributions used to model the nonpartitioning tracer data, where F is the fractional contribution of the second mode. The NAPL saturation distribution parameters f, $\mu_{\ln \hat{S}}$, and $\sigma_{\ln \hat{S}}$ were determined from the partitioning tracer moments using (19)–(21). Domain-average NAPL saturations, $\bar{S}_N$, were determined from measured first moments using (4) and (5), and from the distributed model parameters using (3) and $\bar{S}_N = f\bar{S}_c/(1 + \bar{S}_c)$. Model-determined moments were very close to the measured values (generally within 1%).

of the distributed binary model closely matched the measured data.

[78] For both studies, accurate modeling of the nonpartitioning tracer transport required the superposition of two lognormal distributions; the resulting lognormal parameters are listed in Table 4. Because of the bi-continuous nature of the nonpartitioning tracer BTCs, algebraic solution of (19)–(21) was not possible for these data. The NAPL saturation distribution parameters (Table 4) were determined from (19)–(21) by minimizing the RMSD between the measured and estimated partitioning tracer first three normalized temporal moments. In the absence of data supporting a correlation between K and S_N, $\rho_{t,\hat{S}} = 0$ was assumed for both field sites.

[79] The relatively small $\sigma_{\ln \hat{S}}$ values that were determined for both field sites indicated that, within the contaminated zone, the NAPL saturation distributions were not particularly variable. It, therefore, should not be surprising that application of the homogeneous binary model to these data produced model fits (not shown) that were similar to those presented in Figure 15, with NAPL distribution parameters that were consistent with those in Table 4 (f = {1.0, 0.44, 0.51}, $\bar{S}_N$ = {0.056, 0.003, 0.004} for Hill AFB and Jacksonville RWs 3 and 7, respectively). These data suggest that accurate characterization of nonpartitioning tracer transport (e.g., through the superposition of multiple transport equations) and the fraction of the domain that is contaminated (using either the homogeneous or distributed binary models) may be sufficient to adequately characterize partitioning tracer transport, and thus the NAPL saturation distribution, even when the impact of other factors such as nonequilibrium partitioning and correlations between K and S_N are ignored. Finally, it is emphasized that the estimated f values for both sites were consistent with qualitative expectations based on the type of NAPL and the flow geometry at each site.

6. Discussion and Conclusions

[80] The application of moment equations derived from one-dimensional solute transport models to BTCs generated from multi-dimensional transport processes, as was done here, results in parameters that are representative of equivalent one-dimensional processes. An alternative approach for relating BTC moments to parameters that are descriptive of multi-dimensional transport processes is the stochastic Lagrangian framework that has been developed to consider nonreactive and reactive solute transport in multi-dimensional heterogeneous porous media [e.g., *Dagan*, 1989; *Cvetkovic and Shapiro*, 1990; *Bellin et al.*, 1993; *Cvetkovic et al.*, 1998; *Demmy et al.*, 1999].

[81] The appeal of the Lagrangian approach is that nonreactive and reactive tracer BTC moments can be estimated a priori based on statistics that describe the point variability of the media and contaminant properties, with the presumption that these statistics can be estimated through point sampling. Here, conversely, the focus is on the inverse problem of estimating unknown media and NAPL saturation distribution parameters from tracer BTCs. The models described above allow for the determination of the distribution of travel times and NAPL saturations between streamtubes, not the point distribution. Therefore, the relationship between point and trajectory-average variability was investigated using

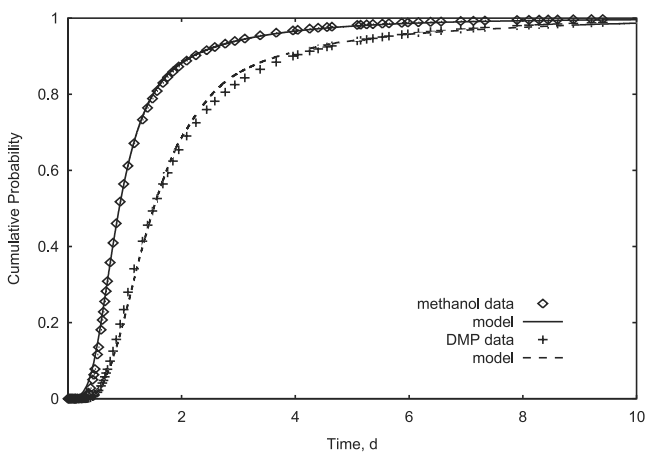

Figure 15. Hill AFB, UT, site measured nonpartitioning and partitioning tracer CDFs with bi-lognormal superposition and distributed binary model fits, respectively.

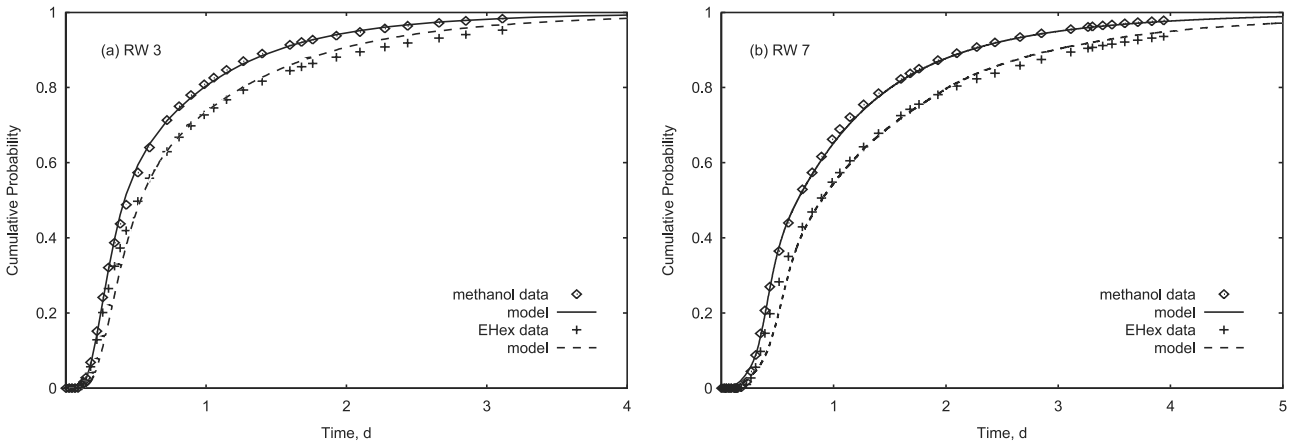

Figure 16. Jacksonville, FL, site measured nonpartitioning and partitioning tracer CDFs with bi-lognormal superposition and distributed binary model fits, respectively, for (a) RW 3 and (b) RW 7.

simulations conducted for a range of flow field variances. Linear variability dampening was observed for $\sigma^2_{\ln K}/\sigma^2_{\ln t,np}$ and $\sigma^2_{\ln S}/\sigma^2_{\ln \hat{S}}$ and the degree of dampening was independent of system variability, with ratios of 0.16 and 0.29 for these two relationships, respectively.

[82] The laboratory experiments investigated the relative contributions of nonuniform NAPL distribution, partitioning isotherm nonlinearity, and nonequilibrium partitioning to excess spreading of partitioning tracer BTCs. Partitioning isotherm nonlinearity appeared to have minimal effect over a tracer concentration range of approximately 3% to 18% of aqueous solubility. The effects of nonequilibrium partitioning, however, were observed over a broad range of pore water velocities. Generally, local conditions are closer to equilibrium at lower velocities and excess spreading due to nonequilibrium partitioning decreases. However, as velocities approach zero, the effects of molecular diffusion become non-negligible. In cases where the NAPL distribution is nonuniform, tracer concentration gradients may exist across streamtubes leading to enhanced BTC spreading from molecular diffusion. Because partitioning rate constants are a function of K_N, the velocities required to achieve local equilibrium will be different for different tracers. Therefore, when multiple partitioning tracers are used in systems with nonuniform NAPL distributions, it is probable that some degree of nonequilibrium effects, on either a local (i.e., pore) or multiple streamtube scale, can be expected regardless of velocity.

[83] In the laboratory experiments, the NAPL was relatively homogeneously distributed within the contaminated zone, but because of nonequilibrium effects the distributed binary model provided better fits to the data than the homogeneous binary model. In these cases, the estimated parameter $\sigma_{\ln \hat{S}}$ is not strictly representative of the standard deviation of the NAPL saturation distribution, but rather can be considered as a general measure that accounts for the spreading of the partitioning tracer BTC. Similarly, for complex applications such as field experiments, it is suggested that $\sigma_{\ln \hat{S}}$ should be interpreted as a parameter that incorporates the combined effects of nonuniform NAPL distribution within the contaminated fraction of the domain, nonequilibrium and nonlinear partitioning, and correlation between NAPL saturation and media properties.

[84] It is emphasized that the methodology presented here requires reliable estimates of tracer BTC moments. Sources of error in moments determined by numerical integration of real data include data gaps, experimental error, and BTC truncation. These effects become particularly significant when estimating higher moments. Obtaining complete moment estimates from model fits to incomplete measured data, as was done here, is one way to overcome these problems; however, as with any parameter estimation technique, the accuracy of the estimated model parameter values is primarily dependent on the appropriateness of the selected model.

[85] For all cases considered here, estimates of the domain contaminated fraction f made using both the homogeneous and distributed binary models were close to measured or anticipated values. Extension of partitioning tracer analyses to include higher moments enables the fraction of the tracer swept volume that is contaminated to be ascertained. For remediation scenarios, *a priori* estimates of the amount of remedial fluids that will be delivered to portions of the domain that contain no NAPL may allow more accurate estimates of expected remediation efficiency. Also, more efficient aquifer remediation system designs may be promoted in cases where knowledge of f is coupled with supplemental information (such as lithological logs or multilevel sampler data) supporting the identification of specific contaminated regions. Determination of NAPL saturation distributions within contaminated zones may also be useful; however, because the models described here are based on the assumption of instantaneous partitioning, our ability to estimate parameters describing these distributions may be restricted until nonequilibrium effects are specifically considered.

[86] **Acknowledgments.** This research was supported by the Florida Agricultural Experiment Station and a grant from the Air Force Office of Scientific Research and approved for publication as Journal Series R-08952.

References

Abu-Dayya, A., and N. C. Beaulieu, Outage probabilities in the presence of correlated lognormal interferers, *IEEE Trans. Veh. Technol.*, *43*(1), 164–173, 1994.

Aitchison, J., and J. A. C. Brown, *The Lognormal Distribution*, Cambridge Univ. Press, New York, 1957.

Annable, M. D., P. S. C. Rao, K. Hatfield, W. D. Graham, A. L. Wood, and C. G. Enfield, Partitioning tracers for measuring residual NAPL: Field-scale test results, *J. Environ. Eng.*, *124*(6), 498–503, 1998.

Atkinson, K., *Elementary Numerical Analysis*, John Wiley, New York, 1985.

Barton, A. F. M., *Alcohols with Water*, Pergamon, New York, 1984.

Bellin, A., A. Rinaldo, W. J. P. Bosma, S. E. A. T. M. van der Zee, and Y. Rubin, Linear equilibrium adsorbing solute transport in physically and chemically heterogeneous porous formations: 1. Analytical solutions, *Water Resour. Res.*, *29*(12), 4019–4030, 1993.

Bosma, W. J. P., A. Bellin, S. E. A. T. M. van der Zee, and A. Rinaldo, Linear equilibrium adsorbing solute transport in physically and chemically heterogeneous porous formations: 2. Numerical results, *Water Resour. Res.*, *29*(12), 4031–4043, 1993.

Cain, R. B., G. R. Johnson, J. E. McCray, W. J. Blanford, and M. L. Brusseau, Partitioning tracer tests for evaluating remediation performance, *Ground Water*, *38*(5), 752–761, 2000.

Cvetkovic, V. D., and A. M. Shapiro, Mass arrival of sorptive solute in heterogeneous porous media, *Water Resour. Res.*, *26*(9), 2057–2067, 1990.

Cvetkovic, V., G. Dagan, and H. Cheng, Contaminant transport in aquifers with spatially variable hydraulic and sorption properties, *Proc. R. Soc. London, Ser. A*, *454*, 2173–2207, 1998.

Dagan, G., *Flow and Transport in Porous Formations*, Springer-Verlag, New York, 1989.

Demmy, G., Solute transport in heterogeneous porous formations, Ph.D. dissertation, Univ. of Fla., Gainesville, 1999.

Demmy, G., S. Berglund, and W. Graham, Injection mode implications for solute transport in porous media: Analysis in a stochastic Lagrangian framework, *Water Resour. Res.*, *35*(7), 1965–1973, 1999.

Falta, R. W., C. M. Lee, S. E. Brame, E. Roeder, J. T. Coates, C. Wright, A. L. Wood, and C. G. Enfield, Field test of high molecular weight alcohol flushing for subsurface nonaqueous phase liquid remediation, *Water Resour. Res.*, *35*(7), 2095–2108, 1999.

Haas, C. N., Moment analysis of tracer experiments, *J. Environ. Eng.*, *122*(12), 1121–1123, 1996.

Helms, A. D. Jr., Moment estimates for imperfect breakthrough data: Theory and application to a field-scale partitioning tracer experiment, M.E. thesis, Univ. of Fla., Gainesville, 1997.

James, A. I., W. D. Graham, K. Hatfield, P. S. C. Rao, and M. D. Annable, Optimal estimation of residual non-aqueous phase liquid saturations using partitioning tracer concentration data, *Water Resour. Res.*, *33*(12), 2621–2636, 1997.

Jawitz, J. W., Aquifer contaminant source zone characterization with partitioning tracers and remediation with single-phase microemulsion flushing, Ph.D. dissertation, 221 pp., Univ. of Fla., Gainesville, 1999.

Jawitz, J. W., M. D. Annable, and P. S. C. Rao, Miscible fluid displacement stability in unconfined porous media: Two-dimensional flow experiments and simulations, *J. Contam. Hydrol.*, *31*, 211–230, 1998a.

Jawitz, J. W., M. D. Annable, and P. S. C. Rao, Using interwell partitioning tracers and the method of moments to estimate the spatial distribution of non-aqueous phase contaminants in aquifers, in *GQ 98 Conference Proceedings, Groundwater Quality: Remediation and Protection*, *IAHS Publ.*, *250*, 422–425, 1998b.

Jawitz, J. W., M. D. Annable, P. S. C. Rao, and R. D. Rhue, Field implementation of a Winsor type I surfactant/alcohol mixture for in situ solubilization of a complex LNAPL as a single-phase microemulsion, *Environ. Sci. Technol.*, *32*(4), 523–530, 1998c.

Jawitz, J. W., M. D. Annable, R. K. Sillan, and P. S. C. Rao, In situ flushing for remediation of aquifer contaminant source zones: Evaluating performance using a control plane approach, in *Proceedings of Contaminated Site Remediation Conference: Challenges Posed by Urban and Industrial Contaminants*, edited by C. D. Johnston, pp. 455–462, Cent. for Groundwater Stud., CSIRO Land and Water, Fremantle, Western Australia, Australia, 1999.

Jawitz, J. W., R. K. Sillan, M. D. Annable, P. S. C. Rao, and K. Warner, In situ alcohol flushing of a DNAPL source zone at a dry cleaner site, *Environ. Sci. Technol.*, *34*(17), 3722–3729, 2000.

Jawitz, J. W., M. D. Annable, C. J. Clark, II, and S. Puranik, Inline gas chromatographic tracer analysis: An alternative to conventional sampling and laboratory analysis for partitioning tracer tests, *Instrum. Sci. Technol.*, *30*(4), 427–438, 2002.

Jin, M., M. Delshad, V. Dwarakanath, D. C. McKinney, G. A. Pope, K. Sepehrnoori, C. E. Tilburg, and R. E. Jackson, Partitioning tracer tests for detection, estimation, and remediation performance assessment of subsurface nonaqueous phase liquids, *Water Resour. Res.*, *31*(5), 1201–1211, 1995.

Jury, W. A., Simulation of solute transport using a transfer function model, *Water Resour. Res.*, *18*(2), 363–368, 1982.

Jury, W. A., and K. Roth, *Transfer Functions and Solute Movement Through Soil*, Birkhäuser Boston, Cambridge, Mass., 1990.

Kabala, Z. J., and G. Sposito, Statistical moments of reactive solute concentration in a heterogeneous aquifer, *Water Resour. Res.*, *27*(3), 759–768, 1991.

Kreft, A., and A. Zuber, On the physical meaning of the dispersion equation and its solutions for different initial and boundary conditions, *Chem. Eng. Sci.*, *33*, 1471–1480, 1978.

Meinardus, H. W., V. Dwarakanath, J. Ewing, G. J. Hirasaki, R. E. Jackson, M. Jin, J. S. Ginn, J. T. Londergan, C. A. Miller, and G. A. Pope, Performance assessment of NAPL remediation in heterogeneous alluvium, *J. Contam. Hydrol.*, *54*, 173–193, 2002.

Nelson, N. T., and M. L. Brusseau, Field study of the partitioning tracer method for detection of dense nonaqueous phase liquid in a trichloroethene-contaminated aquifer, *Environ. Sci. Technol.*, *30*(9), 2859–2863, 1996.

Rao, P. S. C., M. D. Annable, R. K. Sillan, D. Dai, K. H. Hatfield, W. D. Graham, A. L. Wood, and C. G. Enfield, Field-scale evaluation of in-situ cosolvent flushing for remediation of an unconfined aquifer contaminated with a complex LNAPL, *Water Resour. Res.*, *33*(12), 2673–2686, 1997.

Robin, M. J. L., E. A. Sudicky, R. W. Gillham, and R. G. Kachanoski, Spatial variability of strontium distribution coefficients and their correlation with hydraulic conductivity in the Canadian Forces Base Borden aquifer, *Water Resour. Res.*, *27*, 2619–2632, 1991.

Sater, V. E., and O. Levenspiel, Two-phase flow in packed beds: Evaluation of axial dispersion and holdup by moment analysis, *Ind. Eng. Chem. Fund.*, *5*(1), 86–92, 1966.

Schwartz, S. C., and Y. S. Yeh, On the distribution function and moments of power sums with log-normal components, *Bell Syst. Technol. J.*, *61*(7), 1441–1462, 1982.

Sillan, R. K., M. D. Annable, P. S. C. Rao, D. Dai, K. Hatfield, W. D. Graham, A. L. Wood, and C. G. Enfield, Evaluation of in situ cosolvent flushing dynamics using a network of spatially distributed multilevel samplers, *Water Resour. Res.*, *34*(9), 2191–2202, 1998.

Soerens, T. S., D. A. Sabatini, and J. H. Harwell, Effects of flow bypassing and nonuniform NAPL distribution on the mass transfer characteristics of NAPL dissolution, *Water Resour. Res.*, *34*(7), 1657–1673, 1998.

Tompson, A. F. B., Numerical simulation of chemical migration in physically and chemically heterogeneous porous media, *Water Resour. Res.*, *29*(11), 3709–3726, 1993.

Tompson, A. F. B., R. Ababou, and L. R. Gelhar, Implementation of the three-dimensional turning bands random field generator, *Water Resour. Res.*, *25*(10), 2227–2243, 1989.

Valocchi, A. J., Validity of the local equilibrium assumption for modeling sorbing solute transport through homogeneous soils, *Water Resour. Res.*, *21*(6), 808–820, 1985.

Valocchi, A. J., Spatial moment analysis of the transport of kinetically adsorbing solutes through stratified aquifers, *Water Resour. Res.*, *25*(2), 273–279, 1989.

Verschueren, K., *Handbook of Environmental Data on Organic Chemicals*, Van Nostrand Reinhold, New York, 1983.

Willson, C. S., O. Pau, J. A. Pedit, and C. T. Miller, Mass transfer rate limitation effects on partitioning tracer tests, *J. Contam. Hydrol.*, *45*, 79–97, 2000.

Wise, W. R., NAPL characterization via partitioning tracer tests: Quantifying effects of partitioning nonlinearities, *J. Contam. Hydrol.*, *36*, 167–183, 1999.

Wise, W. R., D. Dai, E. A. Fitzpatrick, L. W. Evans, P. S. C. Rao, and M. D. Annable, Non-aqueous phase liquid characterization via partitioning tracer tests: A modified Langmuir relation to describe partitioning nonlinearities, *J. Contam. Hydrol.*, *36*, 153–165, 1999.

Zhang, Y., and W. D. Graham, Spatial characterization of a hydrogeochemically heterogeneous aquifer using partitioning tracers: Optimal estimation of aquifer parameters, *Water Resour. Res.*, *37*(8), 2049–2063, 2001.

J. W. Jawitz, Soil and Water Science Department, University of Florida, PO Box 110290, Gainesville, FL 32611, USA. (jawitz@ufl.edu)

M. D. Annable, Department of Environmental Engineering Sciences, University of Florida, Gainesville, FL 32611, USA.

G. G. Demmy, Layton Graphics, Inc., Atlanta, GA 30062, USA.

P. S. C. Rao, School of Civil Engineering, Purdue University, West Lafayette, IN 47907, USA.